NASA CONTRACTOR REPORT

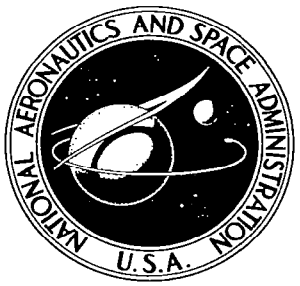

NASA CR-71

NASA CR-751

SURVEY OF DETECTORS AND DYNAMIC CALIBRATION METHODS FOR REMOTE SENSING SYSTEMS

by G. Johnson and A. J. Montgomery

Prepared by
IIT RESEARCH INSTITUTE
Chicago, Ill.
for George C. Marshall Space Flight Center

NATIONAL AERONAUTICS AND SPACE ADMINISTRATION • WASHINGTON, D. C. • APRIL 1967

SURVEY OF DETECTORS AND DYNAMIC CALIBRATION METHODS FOR REMOTE SENSING SYSTEMS

By G. Johnson and A. J. Montgomery

Prepared under Contract No. NAS 8-20107 by
IIT RESEARCH INSTITUTE
Chicago, Ill.

for George C. Marshall Space Flight Center

NATIONAL AERONAUTICS AND SPACE ADMINISTRATION

For sale by the Clearinghouse for Federal Scientific and Technical Information
Springfield, Virginia 22151 – CFSTI price $3.00

FOREWORD

This technical report was prepared by IIT Research Institute, Chicago, Illinois 60616, for the National Aeronautics and Space Administration, George C. Marshall Space Flight Center, on Contract No. NAS8-20107. The program was under the direction of the Fluid Dynamics Research Office with Dr. F. R. Krause as the project monitor.

Personnel who have contributed to this project include M. W. P. Cann, M. J. Fisher, G. Johnson and A. J. Montgomery.

ABSTRACT

The objective of this survey was to provide the data required to choose optimum detectors and calibration systems for use in crossed-beam, cross-correlation measurements. In this application, a pair of intersecting or skew light beams is employed as a non-interfering probe for mapping local thermodynamic properties and turbulent flow characteristics. Fluctuations in number density of either absorbing or scattering media may be studied. For absorption, a narrow spectral bandwidth may be required with consequent limited signal intensity. Detectivity therefore is a parameter of primary concern. Since precision of measurement of correlation function R is a function of light intensity as well as of detectivity, detector signal/noise ratios are presented graphically and algebraically as functions of mean input to the detector. To use these data, mean input is computed from information about a particular source, turbulent fluctuations, and spectrometer, and S/N is obtained from the graphs or equations.

Log-log graphs are used to show slope discontinuities marking successive transitions between dominance of detector noise, signal shot noise, and uncorrelated turbulence noise. Tabulations of mean intensities at these transitions and equations for their calculation are included in the text. In the first region, detectivity is the criterion of precision; in the second, quantum efficiency is the criterion. In the third, precision is independent of either and of source intensity.

TABLE OF CONTENTS

TABLE OF CONTENTS (continued)

LIST OF TABLES

TABLE OF CONTENTS (continued)

TABLE OF CONTENTS (continued)

SURVEY OF DETECTORS AND DYNAMIC CALIBRATION METHODS FOR REMOTE SENSING SYSTEMS

1. INTRODUCTION

This survey of detectors and dynamic calibration methods resulted from the need for optimum detection systems for use in cross beam correlation measurements.[1] Although this survey was directed primarily at detectors for use in cross-beam correlation systems, the information obtained may be applied to remote sensing systems in general. Different types of such systems were discussed in a previous paper by Montgomery et al[2] which should be referred to for details of four methods that can be used for the remote optical sensing of local thermodynamic properties and turbulent flow characteristics. The survey of light sources for cross-beam correlation systems, also carried out under the same contract, NAS8-20107, is described in a separate report which includes a discussion of the optical design of cross-beam systems.

A schematic diagram of a cross-beam correlation system is shown in Figure 1. The wavelength of the radiation must be chosen so that there will be absorption or scattering losses along the beam between the source and the detector systems. The fluctuating signals at the two detectors will be caused by fluctuations in the density of the absorbing or scattering

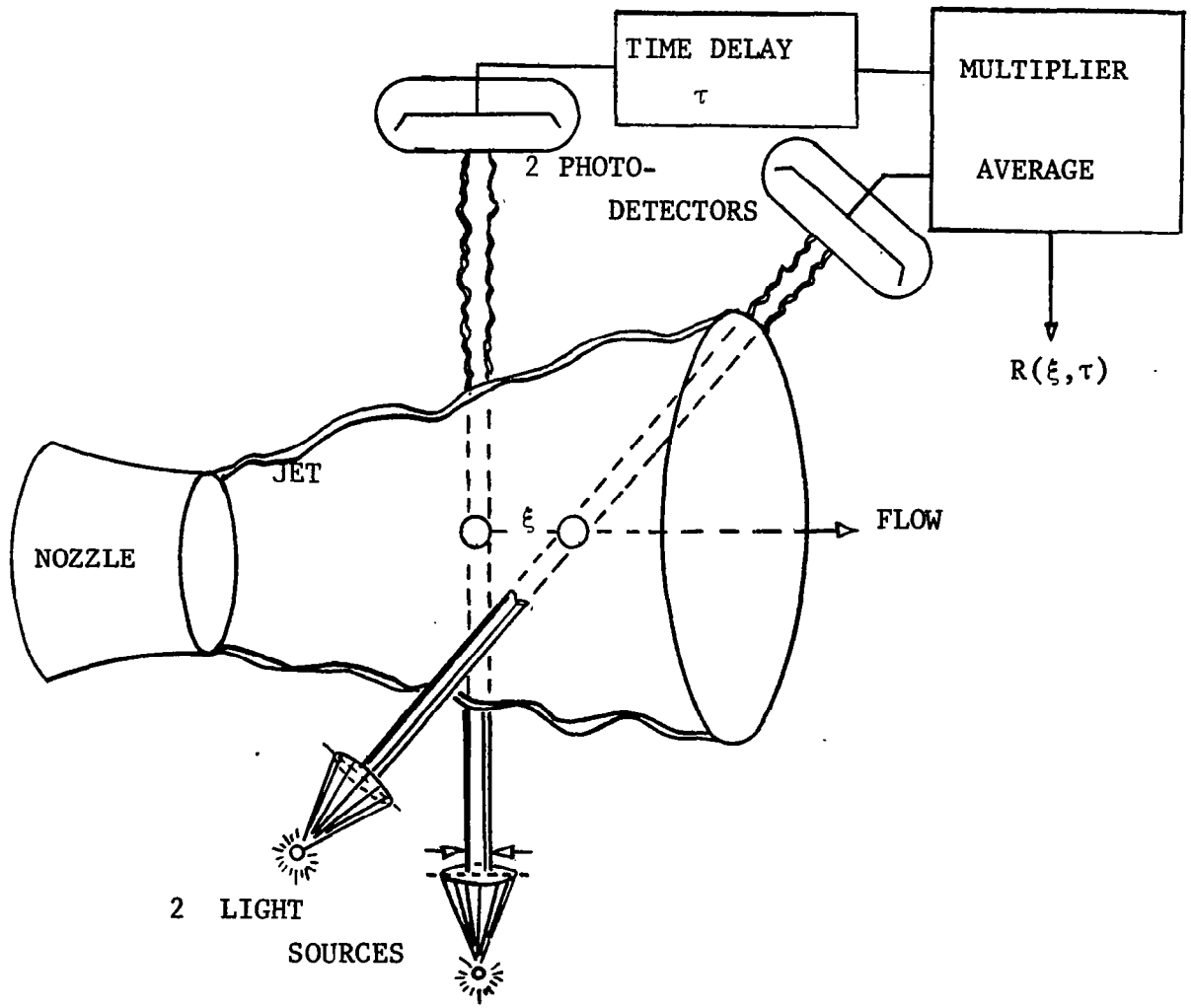

Fig. 1 Cross Beam Correlation Method

particles along the two beams. Each of the detector signals can be considered in two parts, a correlated and an uncorrelated portion. Correlated fluctuations arise from fluctuations in density about the region of overlap of the two beams, and therefore by forming the covariance between the two detector signals these localized density fluctuations may be measured. Uncorrelated fluctuations in the detector output will also be present in the form of detector noise, or noise associated with the signal and thus three different cases may be distinguished which are:

(a) Flow noise limited.

(b) Detector noise limited.

(c) Signal or background noise limited.

Ideally, if sufficiently intense source and sensitive detectors were available, it would be possible to always be limited by the flow noise (a). In practice, however, this may not always be the case, and it is the object of this detector survey to determine, for any given intensity or radiation falling upon the detector, which detector(s) allow the ratio

$$\frac{\text{RMS Level of Correlated Fluctuations}}{\text{RMS Noise}}$$

to be maximized. Since the denominator of this expression includes the noise resulting from uncorrelated density fluctuations along the beam, it will be always less than unity. In general, for low intensity levels at the detector, the denominator

will be determined entirely by the detector noise which is present even in the complete absence of radiation incident on the detector. As the intensity of the incident radiation increases, the RMS noise first remains constant and then begins to increase as the square root of the mean intensity level at the detector. Over the range the output of the detector is linear with input intensity, the rms level of the fluctuations caused by density fluctuations in the flow will increase in direct proportion to the mean intensity level, and thus the point will be reached when the flow noise dominates.

This detector survey determines the most suitable detector to use in a cross-beam correlation system operating at any wavelength or narrow wavelength interval in the range 0.15 to 20 microns. Except in the particular examples discussed it is not possible to specify which of several competing detectors is best at one given wavelength. Additional information is required as to the intensity of radiation incident on the detector and the bandwidth of the fluctuations being measured. However, with a system in which the values of these quantities are known, this report gives the necessary information to determine easily and quickly the most suitable detector.

2. GENERAL DISCUSSION

The variables that must be considered in the evaluation of detectors for use in cross-beam systems are:

(a) Mean intensity of radiation falling on detector.

(b) Distribution of intensity over detector area.

(c) Angular cone of radiation incident upon detector.

(d) Polarization of incident radiation.

(e) Angle of incidence of radiation at detector surface.

(f) Wavelength of radiation.

(g) Frequency content of signal.

(h) Quantum efficienty of detector or its equivalent.

(i) Spectral response of detector.

(j) Variation in sensitivity over area of the detector.

(k) Detectivity or noise equivalent input as a function of frequency (cps).

(l) Frequency response or modulation transfer function.

(m) Phase distortion.

(n) Dynamic range and linearity.

(o) Temporal stability.

(p) Temperature of detector.

Knowledge of the variables (a) through (f) is equivalent to demanding that the radiation falling on the detector be specified in terms of watts/cm^2/steradian/micron as a function of position on the detector surface, wavelength of radiation, and polarization of the incident beam. In a completely general case this information is required because the quantum efficiency or responsivity of the detector is a function of these same variables. However, it is usually sufficient to assume that the detector is illuminated uniformly, at normal incidence with

unpolarized light or light plane polarized in a given direction. Uniform illumination of the detector surface may be achieved if necessary by use of a diffusing plate or other similar device. The detector may always be set perpendicular to the direction of the incident beam, and the f-number of the cone of radiation made greater than two to fulfill the normal incidence condition. Since the change in detector response with the polarization of the incident beam is usually only significant for non-normal incidence, this can likewise be ignored. Thus, only the total power incident on the detector and the wavelength of this radiation need to be specified.

Since usually the quantum efficiency of the detector is specified as a function of wavelength, only for unpolarized light at normal incidence, and usually as an average figure over the sensitive area of the detector, this figure has been used in the survey. In a few cases, the variation in sensitivity over the surface of the detector is given; for example, Electro-Mechanical Research supply this information with each individual photomultiplier but, in general, this is not part of the specifications supplied by detector manufacturers.

The detectivity or noise equivalent input is usually given by the detector manufacturer as a function of frequency, and the responsivity is similarly specified. Phase distortion information was never supplied and is unavailable; however, detectors which have a very fast response to changes in the illumination level will not present a problem and, in the case of slower

detectors, matched systems may be used. Provided the detector is linear, the cross-correlation obtained with two detectors with similar phase characteristics will be identical to the result for detectors with zero phase shifts for all frequencies. The dynamic range and linearity depend on the conditions of operations and are discussed in later sections of this report.

3. CONSIDERATIONS RELATING TO OPTICAL SYSTEM DESIGN

The design of the optical system used in applications of the cross-beam technique has to maximize the radiation throughput while maintaining the required beam diameter, beam collimation and spectral bandwidth. The optical design of cross-beam systems has been discussed in some detail in the report on light sources, and thus will only be briefly mentioned here. Usually, as shown in Figure 2, there will be a lens or mirror system which focuses the incident radiation onto a small aperture that determines the beam collimation or limits the field of view of the system. This aperture is followed by a monochromator or a filter which limits the spectral bandwidth of the radiation incident on the detector. The monochromator entrance aperture will usually be at least as big as the entrance aperture which, for maximum light throughput, will be determined solely by the beam collimation requirements. If, with a particular monochromator, the spectral bandwidth dictates a narrower entrance aperture than that based on the desired beam collimation, then the light throughput will be reduced. However, if the linear

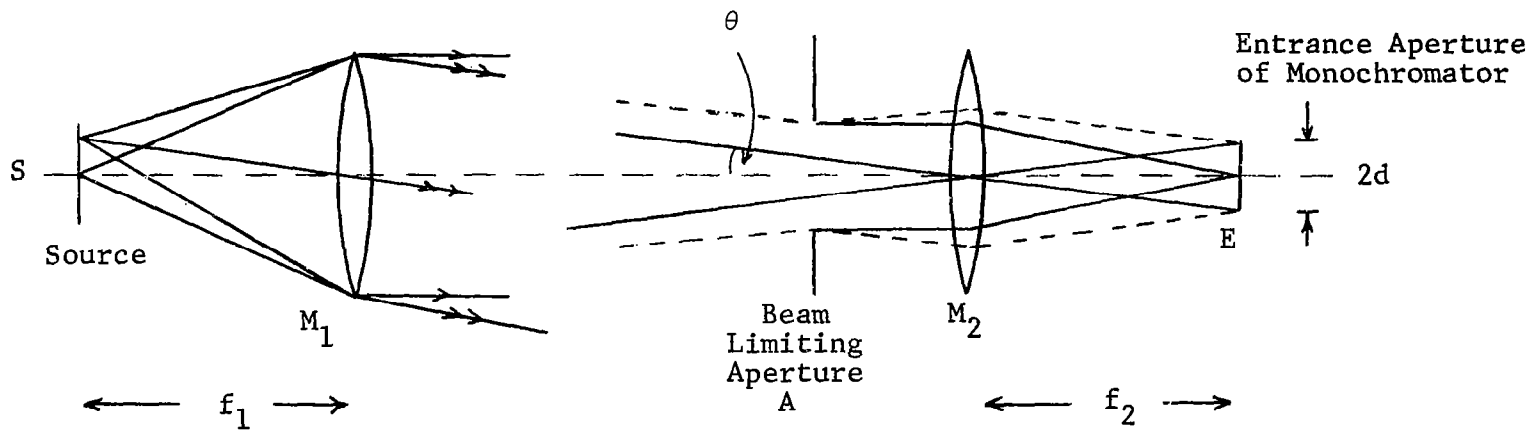

FIG. 2 SCHEMATIC DIAGRAM OF OPTICAL SYSTEM

dispersion of the monochromator is increased by changing the grating, then a decrease in width of the entrance aperture will not be necessary. Alternatively, if the f-number of the monochromator is less than the f-number of the cone of radiation incident on the entrance aperture, that is, if

$$\text{f-number of monochromator} < \frac{f_2}{D}$$

then both the focal length f_2, and the diameter of the entrance aperture may be made smaller. Provided that both are reduced proportionally, the beam collimation and light throughput will be unaffected. Typical figures are:

Monochromator f/7	0.5 meter
Beam Diameter D	2 mm (Model Air Jet)
	20 mm (Full scale static firing)
Beam Collimation	3 arc minutes

The monochromator f-number and the beam diameter together determine the minimum focal length of lens, L_2, which will be 14 mm and 140 mm for these two cases leading to monochromator entrance apertures of 10 or 100 microns, respectively.

If a focused beam system is used the monochromator entrance aperture can be much larger. The spectral bandwidth, unless this is very broad, may then limit the monochromator entrance size in a practical case. For example, with a 0.5 meter monochromator using a diffraction grating having 1200 lines per mm, the linear dispersion is 16A per mm. If a spectral bandpass of 50A is desired, then the monochromator entrance and

exit apertures will be approximately 3 mm in diameter. A detector directly behind the entrance aperture would also have to be 3 mm in diameter, but reimaging the exit aperture onto the detector would permit smaller detectors to be used. From optical design considerations, therefore, it will not be necessary for the detector size to exceed 3 mm. The minimum size of the detector will depend on the particular optical system, the spectral bandwidth, beam diameter, etc., but detectors with a minimum size of 1 mm^2 will be adequate for most conditions of operation.

4. DETECTOR SPECIFICATIONS

4.1. Introduction

The objective of this detector survey is to determine the most suitable detector to use in a cross-beam system operating at any wavelength or narrow wavelength interval in the range 0.15 to 20 microns. Conventionally this wavelength range divides into three parts:

Ultraviolet	0.15 - 0.38 microns
Visible	0.38 - 0.7 microns
Infrared	0.7 - 20 microns

In the ultraviolet and visible spectral regions, fast detectors are available which are signal-noise limited and, hence, the choice of the most suitable detector is a comparatively simple one. For this reason a large part of the effort on the

survey was directed toward infrared detectors which pose many more problems. There is a great diversity of infrared detector types which are appropriate to various segments of this wide spectral range. However, complete classes of detectors may be omitted from consideration because they have too slow a response to changes in the incident light level. This category includes thermocouples, bolometers and Golay cells.

In order to compare the performance of detectors for use in fluctuation measurements it is necessary to understand the meaning of the terms quantum efficiency, detectivity, transfer function, and linearity, and these concepts are therefore discussed in the following sections.

4.2 Quantum Efficiency

There is no unique definition of quantum efficiency. Many different types have been used in the literature and most of these relate to responsivity and are therefore called responsive quantum efficiency. However, one type, detective quantum efficiency, first formulated by Rose,[3] is of particular importance in connection with the detecting ability of detectors. This concept has been discussed in detail by Jones,[4] and therefore a very cursory treatment will be given here.

Photoemissive tubes are the simplest to discuss in terms of quantum efficiency. If N_i photons of a particular wavelength are incident on the sensitive surface of a photoemissive type of detector and N_e of these are effective in producing the excitation that contributes to the electrical

output, then the quantum efficiency is given by the ratio of the effective to incident quanta, N_e/N_i. In a phototube or photomultiplier, this is equivalent to the number of photoelectrons emitted per incident photon expressed as a percentage.

If two detectors are being compared in performance for use in cross-correlation measurements and the intensity of radiation is sufficient to make both signal noise limited, then assuming both have linear input/output characteristics up to this radiation level, the better detector will be that with the higher quantum efficiency. Of course, if the fluctuations in the detector signal caused by the turbulent flow being studied is larger than other sources of noise, then this will be the limiting factor and the two detectors will be equivalent. Under these circumstances the best detector would be the one most convenient to operate and/or the cheapest.

To determine whether or not a detector is signal-noise limited, it is necessary to compute the noise associated with the signal and compare this with other sources of noise; thus, in the case of a photomultiplier with a quantum efficiency q, the photocurrent is given by

$$i_s = Neq$$

where e = electronic charge = 1.6×10^{-19} coulombs and N is the mean number of photons incident per second. In addition to the photocurrent, there is also the dark current, i_d, which occurs in the absence of any radiation falling on the detector, and thus

the total cathode current is given by

$$i_o = i_s + i_d .$$

The fluctuations in i_o due to the random arrival of photons at the cathode and the random emission of both the photoelectrons and the dark current electrons are

$$\overline{i^2}_n = 2ei_o (f_2 - f_1)$$

where $\overline{i^2}_n$ is the noise power and $(f_2 - f_1)$ is the electronic bandwidth. The mean signal to rms noise at the cathode is, therefore,

$$\left(\frac{S}{N}\right)_{\text{cathode}} = \left[\frac{i_o}{2d(f_2 - f_1)}\right]^{1/2} .$$

The dynode chain amplification in a photomultiplier introduces relatively little additional noise. The theory of such noise is developed in a fundamental paper by Shockley and Pierce.[5] They find that if:

(1) the noise in the cathode current is shot noise

(2) at each dynode the number of secondary electrons for each primary electron has a Poisson distribution

(3) the gain of each dynode is the same

then the amplification process increases the mean square noise more than the signal squared by the factor

$$\frac{Mm-1}{M(m-1)} ,$$

where M is the total gain of the dynode chain and m is the gain of each dynode. Practically, these assumptions are well met and, since M is very large, the factor reduces to

$$\frac{m}{m-1}$$

Since m is typically of the order of 2.7 (10^6 gain in a 14 stage tube) the mean signal/rms noise ratio at the anode is decreased by a factor of 1.26 times its value at the cathode.

In the case of cross-correlation measurements on supersonic jets where fluctuations, which are a small percentage of the mean signal level, are correlated between two detectors, it is highly desirable that the mean signal/rms noise ratio be at least 10. The bandwidth of fluctuations is wide ($\sim$ 50,000 cps), and thus to obtain S/N = 10 the cathode current will have to be

$$i_o \sim 8 \times 10^{-13} \text{ amperes.}$$

In calling the mean current the signal, it has been tacitly assumed that the dark current i_d is small compared with the photocurrent i_s; thus,

$$i_o \simeq i_s .$$

For a typical photomultiplier such as the RCA 6903, the dark current is 3×10^{-16} amperes and thus this approximate equality is well satisfied.

Note that in this condition of operation the performance of the detector is not at all dependent on the area of the photocathode. If the photocathode is made smaller and the radiation concentrated in a smaller area, then no change will be produced in the S/N ratio.

In the case of photoconductive cells which were shown in this survey to be, with few exceptions, the optimum type of detector for use in the infrared region of the spectrum, the situation is entirely different. It is difficult to make the photon noise dominant in the output of a lead sulfide cell whereas as explained above the photon noise is usually dominant in the output of a multiplier phototube. Another marked difference is that in many, if not most infrared systems, the signal is chopped, and either a narrow band electronic amplifier or synchronous detection technique is used. There is usually some optimum chopping frequency which will give the best signal/noise ratio, which is commonly of the order of a few hundred cycles per second.

Background radiation is usually of much greater significance in infrared systems than in systems operating in the ultraviolet and visible regions of the spectrum. Thus, some detectors useful at the larger wavelengths (10-20μ) are background noise limited. The background is usually at a temperature of 300°K, and the peak of the blackbody curve at this wavelength is at approximately ten microns. If the source radiation is predominantly at some wavelength, λ, a common approach to limit

the background radiation falling on the detector is to use a filter which passes radiation at wavelength λ and is opaque to wavelengths outside a band of width $\Delta\lambda$ centered on wavelength λ. This does no good in infrared systems if the filter is at the same temperature as the background since it will radiate in the spectral regions where it is opaque just as does the background. Thus, a cooled filter has to be used for an improvement to be realized.

If a monochromator is used and the background radiation is the factor limiting the performance of the system, then the detector should be situated in a cooled cell which limits the field of view of the detector to that of the cone of radiation impinging upon it from the optical element in front of it. It is probably not necessary to cool the mirrors and grating in the monochromator because of their high reflectivity, but a large improvement can result from cooling the area to either side of the entrance slit from where radiation may be diffracted by the grating onto the detector.

Returning to the particular topic under discussion, that of the quantum efficiency of photoconductive cells, we note that very few measurements have been made of this quantity. However, because of the nature of cross-correlation technique applied to fluctuation measurements, where we wish to correlate small fluctuations in intensity of a powerful beam of radiation, a detector is quite likely to reach the signal noise limited condition. Hence, a knowledge of the quantum efficiency is needed

if the point at which the detector becomes signal noise limited is to be known.

The measurement of small fluctuations in intensity of a powerful beam of radiation is equivalent to the problem of measuring small fluctuations against a large background. This 'background' level does need to be known, however, because the magnitude of the fluctuations will be directly proportional to the intensity of the beam.

The detective quantum efficiency (DQE) of a photoconductive element is defined as the number of electron-hole pairs produced per incident photon. Thus, the DQE cannot be greater than the absorptance. Antireflection films may be used to increase the absorptance, especially in materials having a high index of refraction.[6] The responsive quantum efficiency (RQE), on the other hand, is based on the absorbed photons, and hence can have a maximum value of unity. In fact, the hypothesis that all photoconductors that have a sharp absorption edge have an RQE of unity for wavelengths just shorter than the edge and for some distance toward shorter wavelengths has come to be widely accepted by solid-state physicists, and was proved experimentally by Goucher,[7] for intrinsic germanium. It is easy to understand the basis of this hypothesis: at the short wavelength side of the absorption edge, the absorption coefficient increases by several orders of magnitude. This absorption increase is due to the much increased cross section for pair production. Thus, if the absorption coefficient is increased by three orders of

magnitude, all but one part in 10^3 is due to pair production. This is equivalent to saying that 99.9% of the absorbed photons produce pairs, and the RQE is therefore 99.9%.

However, as Rose[8] has pointed out, in a photoconductive cell, there is a statistical fluctuation in the number of free carriers and also in their lifetime. These two fluctuations contribute equally to the mean square noise voltage in the output. The result is that the mean-square noise in the output, when referred to the input, is never less than twice the noise in the steady incident radiation. Therefore the effective DQE can never exceed 0.5.

To determine whether a detector is signal or background noise limited, the number of signal photons and the number of background photons, of shorter wavelength than the absorption edge, falling on the detector have to be calculated. If the number of signal photons exceeds the number of background photons, then the detector will be signal noise limited and vice versa. This assumes that other noise sources are small compared to the background and/or signal noise. In fact, many photoconductive detectors are current noise limited even for incident radiation levels that would produce output signals several thousand times the rms noise level in a bandwidth of 50,000 cps.

The fluctuations in a detector output signal due to detector noise (current or thermal noise) or background noise (usually included assuming a field of view of 2π radians and a

blackbody background at a temperature ~ 295°K) may be calculated directly from the detectivity of the detector which is specified by the manufacturer. Noise produced by the signal radiation may be calculated as follows. If $\overline{N}$ is the average arrival rate of photons of wavelength λ at the detector, then, since the emission of photons from the source is a random process, the mean square deviation in the rate of arrival $\overline{N^2}$ will be equal to $\overline{N}$. The frequency dependence of the mean square fluctuations in the rate of generation of current carriers due to the arrival of the signal photons is therefore given by

$$P_n(f) = \int_{\Delta\lambda} \eta(\lambda)\, \overline{N} d\lambda$$

where η is the quantum efficiency and the integration is over the spectral band of the radiation. In practice, the dependence of η on wavelength may be ignored so that

$$P_n(f) = \eta_o \overline{N}$$

The rms fluctuations in bandwidth Δf is then given by

$$n_s = [P_n(f) \cdot 2\Delta f]^{1/2} = [\eta_o\, 2\Delta f\, \overline{N}]^{1/2} .$$

From the differential responsivity of the photoconductive cell, the output fluctuations can then be found and compared with fluctuations produced by other noise sources. Alternatively,

since the noise equivalent input is available directly from the detectivity, an immediate comparison may be made. This latter technique will lead to erroneous results if the detector becomes nonlinear at these levels of incident radiation.

Although generally photoconductive cells have higher detectivities than their photovoltaic or photodiode counterparts, the latter have higher quantum efficiencies, and hence for high incident intensity levels may be preferred in some cases. In photovoltaic cells used as photodiodes the electron-hole pair produced separate under the action of the electric field resulting in a transfer of electric charge between electrodes. Since the effect of fluctuation in carrier lifetime is absent, the detective quantum efficiency has a maximum value of unity in contrast to 0.5 in the photoconductive case.

4.3 Spectral Response

The relative response of a detector as a function of wavelength is usually given on specification sheets supplied by the detector manufacturer but, if not, this information may be readily obtained. The method of presentation varies with different types of detection, and with different manufacturers. Although, with quantum type detectors, it would seem to be logical to graph the relative response for some number of incident photons as a function of wavelength, this is not usually done. Equal energy response curves are much more common. It is for this reason that the spectral response curves of photoconductive cells show a pronounced fall-off at wavelengths

shorter than the absorption edge. On a number of quanta basis, the response curve is quite flat to the cut-off wavelength.

In the case of phototubes or photomultipliers, the quantum efficiency as a function of wavelength is sometimes given; however, there are generally agreed to designations of the spectral response characteristics of some photoemissive devices which apply, irrespective of manufacturer. This S-number designation is the spectral response of a device, not of a photocathode per se, and includes the transmission of the window material. Thus, a tube with an S-11 response becomes an S-13 with a fused quartz window, and although there are no further type designations, the same photocathode material, a combination of antimony and cesium, gives a quantum efficiency of better than 10% down to approximately 1100A when a LiF window is used.

With infrared detectors the spectral response is often given in terms of the detectivity as a function of wavelength. Since the detectivity is related to the noise in the detector output as described in section 4.4, if the noise level is constant then the detectivity vs. wavelength curve will be precisely the same as a curve giving the relative response vs. wavelength. The assumption of a constant noise level will be valid for detector noise or where a detector is background noise limited. If the point is reached when noise associated with the signal itself is significant then detectivity vs. wavelength and spectral response vs. wavelength curves cannot be used interchangeably.

In cross-beam correlation measurements, general spectroscopic considerations indicate the relevance, in certain experiments, of measuring the integrated intensity of groups of bands with a total width of as much as 1% of the center wavelength. Therefore, it is highly desirable for the spectral response characteristic of the detector to show no fine structure within 1% intervals. This smooth, featureless condition is generally met by detectors. Occasionally, periodic ripples are seen superimposed on spectral response curves of experimental infrared detectors, caused by optical interferences in the window. The effect is readily detected by running the curve. As noted above, spectral response curves are traditionally presented on an equal power per unit bandwidth basis despite a general tendency among non-thermal detectors to show a flat response on an equal photon density per unit bandwidth basis, with a rather sharp long-wave cut-off. The cut-off is usually defined as the wavelength at which the equal power response is half the peak value.

4.4 Detectivity

The detectivity of a detector, a concept introduced by Jones,[9] is of particular importance in comparing the performance of infrared detectors and, in fact, forms the main basis of comparison in choosing suitable detectors for use in cross-beam or cross view experiments. It is related to the Noise Equivalent Input (NEI) which is defined as the rms radiation input which will produce an r.m.s. signal-to-noise ratio of unity.

This assumes that incident radiation is chopped at some given frequency, and is usually specified for a 1 cps electronic bandwidth. The detectivity (D) is the reciprocal of the NEP, that is,

$$D_\lambda = \frac{R_v}{\text{r.m.s. noise output of cell}}$$

where $$R_v = \frac{\text{r.m.s. output voltage}}{\text{r.m.s. power incident upon detector}}$$

R_v, the responsivity is measured in r.m.s. volts per r.m.s. watt.

Since most detectors exhibit a noise equivalent power which is directly proportional to the square root of the area of the detector, an area independent figure of merit can be obtained by dividing the NEI by the square root of the area. This leads to a detectivity, D* ("dee-star") given by

$$D^*_\lambda = \frac{1}{NEI\ A^{-1/2}}$$

where A is the area of the detector. D* is, in fact, the widely used figure of merit, and it has become common usage to refer to D* as the detectivity. The units of D* are $cm(cps)^{1/2}/watt$, and the reference bandwidth is always 1 cps.

D^*_λ is a function of wavelength, as denoted by the subscript λ, and the exact functional dependence is usually specified by the detector manufacturer. For typical spectral

bandwidths applicable to cross-beam measurements, $\Delta\lambda < \frac{\lambda}{100}$, and it will usually be adequate to use the detectivity figure appropriate to the center wavelength, λ.

The detectivity is also a function of the chopping frequency used in its measurement. Since the cross beam technique has by its very nature to deal with a broad bandwidth of fluctuations, typically from 100 to 50,000 cps, this variation in detectivity has to be taken into account. This information is usually supplied by detector manufacturers in the form of log-log plots of D* in cm. $cps^{1/2}$/watt vs frequency as shown in Figure 3. Such curves may be regarded as inverted plots of the rms noise spectrum after equalization to a flat signal response. Mean square values may be obtained by expanding the ordinate scale two-fold. These doubled curves may then be integrated by piecewise linear approximation between 100 and 50,000 cps. Since they often consist only of two segments, at low frequencies increasing directly with frequency reaching a plateau value at high frequencies, this is easily accomplished. If the plateau is reached at a frequency of less than 10,000 cps then little error will occur if comparisons between different detectors are made on the basis of the plateau value of the detectivity.

The reason for the decrease in detectivity at low frequencies is the predominance of current noise, or 1/f ("one over f") noise, as it is often called. Its power spectrum is characterized by an approximate dependence upon the reciprocal

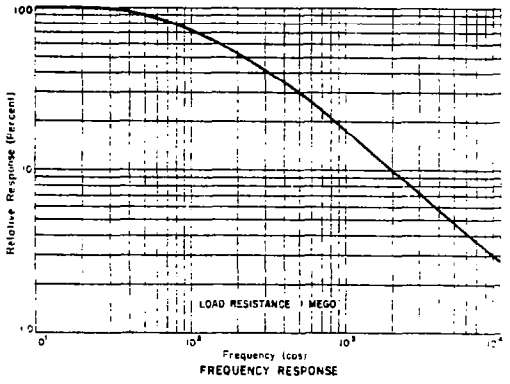

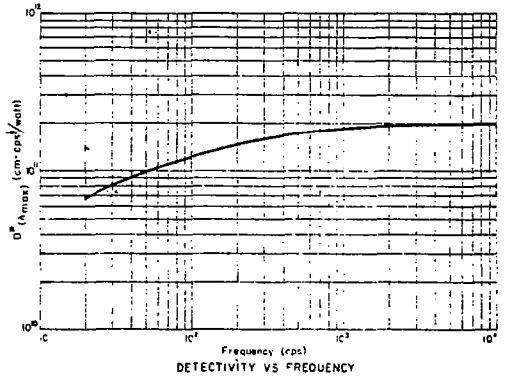

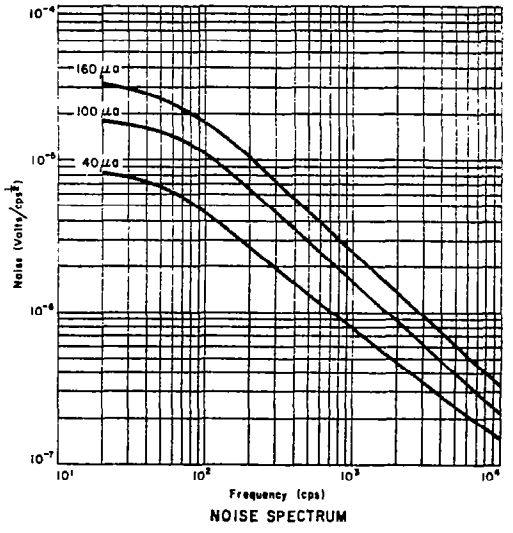

Fig. 3 NOLC Frequency Response Determination of a Lead Sulfide Detector by Santa Barbara Research Center

of the frequency and the square of the current. At higher frequencies generation recombination noise becomes dominant, characterized by a power spectrum which is constant at low frequencies, but decreases rapidly beyond a characteristic frequency related to the inverse of the carrier lifetime. Since the response of the detector is similarly related to the carrier lifetime, this explains why a constant detectivity is maintained out to frequencies where the response of the detector may have fallen by a factor of 100.

4.5 Transfer Function

For accurate interpretation of the results obtained in the cross correlation of the two detector signals in cross beam or cross view experiments, it is necessary for the two detecting systems to have similar transfer function characteristics, and that their frequency responses or modulation transfer functions be flat over the frequency range of interest. Phase differences between the two channels cannot be tolerated, but phase changes varying with signal frequency which are similar for both detector systems are acceptable. It is desirable, however, that this phase change with frequency be small over the frequency range of interest, so that the possibility of a significant phase difference occurring due to environmental change is minimized.

Over most of the spectral wavelength range of interest in this survey, that is, from 0.15 to 20 microns, the most suitable detectors have response times in the microsecond or

submicrosecond region. Such detectors have transfer functions which are wholly real and essentially equal to unity up to and exceeding 50,000 cps which is the maximum frequency of interest.

It is in the spectral region from one to about six microns where detectors with the highest detectivities also have responsivities which begin to decrease at quite low frequencies, of the order of 1,000 cps in some cases. However, there is usually a corresponding decrease in noise per unit bandwidth, and therefore the detectivity changes very little. A typical example is given in Figure 3. Provided that the signal/noise ratio is maintained up to 50,000 cps, then the use of an electronic amplifier with an inverse characteristic will produce an output equivalent to that given by a detector with a flat frequency response characteristic and a flat noise spectrum. It is therefore important not to rule out of consideration any detector solely on the basis of its poor responsivity at the higher frequencies of interest.

4.6 Dynamic Range and Linearity

The dynamic range and linearity requirements to be placed on the detecting systems for use in crossed-beam experiments are dependent upon the magnitude of the fluctuations being measured. It is desirable that these fluctuations be large compared with detector noise and signal or background shot noise. To achieve this condition, the mean power incident upon the detectors may have to be large, and therefore a wide dynamic range is required.

In order to consider a concrete example, it is assumed throughout this report that the rms value of the fluctuations which are correlated between the two detectors is 1% of mean signal level. If the rms value of the detector noise, together with the signal and background shot noise, is of this same order of magnitude, then the integration time necessary to give any required experimental accuracy will be determined by the fluctuations in intensity of the radiation incident upon the detectors that are uncorrelated. These uncorrelated fluctuations have previously been referred to as flow noise. Their magnitude depends on the correlation length or eddy scales in the flow, and on the physical extent of the flow field. Again, for the purpose of discussion in this report, it will be assumed that these are of the order of ten eddies along either of the crossed beams, and thus the rms flow noise will be $\sim \sqrt{10}$ x 1% or 3.3% of the mean signal level.

Because the fluctuating signals have an amplitude that is only a small percentage of the mean intensity level, precise linearity of detector output with light intensity is not necessary. If the detector system introduces less than 5% harmonic distortion for a sinusoidal input signal that is equal in amplitude to the rms amplitude of the fluctuating signal, then the system will be suitable, on the basis of linearity, for crossed-beam experiments. In fact, in cases where the fluctuations are small, it would be possible for the detector to saturate without exceeding this tolerance.

Practically then, it will be the differential responsivity which will usually set a limit on the detector nonlinearity. As saturation is approached, the change in output signal for a 1% change in input beam intensity will decrease in relation to the noise, and in this case, an improved signal/noise ratio will be obtained by decreasing the intensity of the incident radiation.

The dynamic range specification for a detector, to be most useful, has to be defined in similar terms. A dynamic range of at least 100 is required; thus, the rms amplitude of the output signal produced by a 1% fluctuation in the radiative power input, excluding the background radiation, should be equal to or greater than the rms noise output in a bandwidth 100 to 50,000 cps.

5. EFFECT OF NOISE ON INTEGRATION TIME

In considering ways of presenting the detector data to include cases where the accuracy is limited by uncorrelated portions of the detector signal arising from the flow, the effect of integration time on the accuracy of the measured correlation coefficient was investigated. If the fluctuating signals at the two detectors are given by

$$i_1 = i_{1c} + i_{1u}$$

$$i_2 = i_{2c} + i_{2u}$$

where the subscripts c and u indicate the correlated and uncorrelated portions of the signal, respectively, then the correlation coefficient, r, is given by

$$r = \frac{\overline{i_{1c}\, i_{2c}}}{\left[\overline{\left(i_{1c} + i_{1u}\right)^2}\ \overline{\left(i_{2c} + i_{2u}\right)^2}\right]^{1/2}}$$

If the two signals are approximately the same level, we can write

$$r = \frac{\overline{i_c^2}}{\overline{i_c^2} + \overline{i_u^2}} = \frac{1}{1 + \dfrac{\overline{i_u^2}}{\overline{i_c^2}}} \quad .$$

There will be an uncertainty in the measurement of r due to the finite integration time. This uncertainty for a typical fluctuation noise spectrum is given by

$$\sigma(T) = \frac{1}{\sqrt{B\,T}} \quad ,$$

where B is the electronic bandwidth and T is the integration time.

To make a measurement of the correlated fluctuations in the presence of shot or detector noise with the same accuracy as when such noise is absent requires that the quotient r/σ remain constant. Using the figure of ten eddies across the flow, the correlation coefficient in the absence of shot and instrument noise would be 0.1. If an integration time, T, is used, then the error in the measured r will be taken to be σ_1.

Now, considering the case where the rms shot or detector noise is 10 times the rms value of the correlated fluctuations that we wish to measure, we have

$$r = \frac{1}{1 + \frac{109}{1}} \approx 0.009 \quad .$$

If the same accuracy is required in the measurement of the correlated fluctuations, then the same percentage accuracy is required in the correlation coefficient. Thus,

$$\frac{\sigma_1}{0.1} = \frac{\sigma_2}{0.009} \, ,$$

or

$$\sigma_2 = 0.09 \, \sigma_1$$

and the integration time to obtain this σ_2 would be $T_2 = 123 \, T_1$. An rms noise level one hundred times the correlated fluctuations that we wish to measure, or ten times greater than the above example, requires a further increase in integration

time by a factor of 10^4, if the same percentage accuracy is to be obtained in the correlation coefficient.

The accuracy could be ultimately determined by the analogue-to-digital conversion in the data processing. With the present RAVAN program, the digitization is good to one part in one hundred and twenty-eight, and therefore the second example above is close to the point of being limited by the A-to-D conversion.

For an accuracy of 5% in the correlation coefficient, the specified maximum integration time of 5 minutes requires a minimum signal/noise ratio of 0.064.

6. DETECTOR DYNAMIC CALIBRATION TECHNIQUES

6.1 Detector Performance Tests

A survey of methods for dynamic calibration of cross-beam correlation systems was carried out on this program. This was preceded by a literature search for calibration methods developed expressly for correlation measurements, especially those with optical inputs. General observations are that published literature is dominated by discussions of the mathematical theory rather than by experiment, that recent papers tend to refer to theoretical discussions circa 1950, that recent literature is contained to a large extent in technical reports of government contractors and, that auto-correlation has been much more commonly exploited than cross-correlation.

Autocorrelation provides no information on detector-amplifier channel matching considerations. In a parallel approach, standard performance tests for sources and detectors were chosen as a useful starting point for such a survey, with the objective of finding in what manner they might be modified for application to cross-correlation measurements on turbulent flows.

Dynamic methods are employed almost exclusively in detector evaluation and, thus, radiation intensities and signal and noise voltages are generally understood to mean root-mean-square values.

The principal performance parameters customarily measured for detectors are detectivity, responsivity, spectral response, frequency response, and/or time constant, and noise spectrum. These terms have specific meanings of wide acceptance; therefore, definitions will be given before the measurement techniques are described.

Responsivity, $\mathcal{R}$, is a measure of the response to stimulus ratio, and is defined to be the ratio of the rms value, S, of the fundamental component of the detector circuit signal voltage to the rms value, Φ, of the fundamental component of the modulated radiation intensity incident on the detector, in volts per watt. Circuit operating conditions must be specified. Some detectors are passive circuit elements and produce no signal voltage; hence, responsivity is generally a property of the detector circuit rather than of the detector. Voltage pre-amplifiers may be built with any desired amplification factor;

if the preamplifier is defined to be part of the detector circuit, the arbitrary nature of any single value for the responsivity of a linear system becomes evident. Responsivity is used to assess linearity and to determine signal-to-noise ratios and detectivity.

Detectivity, D, is the ratio of the responsivity to the rms noise voltage, N, per unit observational bandwidth observed under the same conditions. Thus, $D = S/N\Phi$, and it may be alternatively viewed as the signal-to-noise ratio per watt of stimulus, a specific signal-to-noise ratio. The definition implies that signal and noise are independent, and that the internal noise of the detector is, in practice, the dominant noise. This is the case for most infrared detectors under usual conditions of operation.

Spectral response is the dependence of relative responsivity on wavelength, $\mathcal{R}(\lambda)$. It is usually measured at a modulation frequency less than 100 cps.

Frequency response is the dependence of relative responsivity on modulation frequency, $R(\omega)$, normalized to a plateau value usually observed at low frequencies.

Rise and decay time constants are the respective times for the transient signal voltage to undergo a fraction $(1 - \frac{1}{e})$ of the total change upon abrupt exposure to continuous illumination, and upon abrupt cessation of illumination following attainment of a steady-state value.

Responsivities are usually determined by measurement of the signal voltage resulting from exposure to a modulated source of known absolute power density at the detector. For applications involving a wide spectral wavelength range, such as spectrometry, modulation methods are largely restricted by transmittance problems to rotating sector choppers and rotating mirrors. Methods of responsivity determination tend to reflect this limitation, despite the difficulties in the attainment of high frequencies by mechanical means.

The mechanically modulated systems are usually designed to produce equal on and off times with abrupt transitions, referred to as square-wave chopping. The rms signal voltage, S, is measured in a narrow band centered on the interruption frequency. If the power incident on the detector while the chopper is in the on position is Φ watts, the responsivity is given by

$$\mathcal{R} = \frac{\pi S}{\Phi \sqrt{2}} .$$

The numerical coefficient $\frac{\pi}{\sqrt{2}}$ is the ratio of the peak-to-peak value of a square-wave to the rms value of its fundamental component. The principal advantage of the square-wave form is its ready characterizability from its geometry. Sinusoidal choppers are sometimes constructed in order to obtain an output that is the same for wide and narrow bandwidths. The Naval Ordnance Laboratory, Corona, employs a sinusoidally modulated

Nernst glower for frequencies between 100 and 40,000 cps.

For practical beam cross sections, chopper diameters, and rotational velocities, it is difficult to obtain steep wavefronts much above 1000 cps. Garbuny, Vogl, and Hansen[10] designed a chopper consisting of a hexagonal drum of front-surface mirrors rotating within an array of stationary mirrors arranged to multiply the rate at which the exit beam sweeps past the detector. Fundamental pulse frequencies of 2×10^4 cps have been attained with this arrangement with rise times of 10^{-9} sec.

Frequency response measurements are made alternatively with a square-wave chopper and narrow-band amplifier or sinusoidal chopper and wide-band amplifier, the fundamental modulation component being observed in either case. On the assumption that the dynamic behavior of semiconductor devices is governed by a bimolecular recombination process between major and minor constituents, a simple exponential response is expected to a step function, characterized by a single time constant, τ. In the frequency domain, the corresponding frequency response curve expected is

$$\mathcal{R}(\omega) = \mathcal{R}(0)\left[1 + \omega^2\tau^2\right]^{-1/2}$$

where ω = fundamental frequency, radians/sec

$\mathcal{R}(0)$ = limit of responsivity as ω approaches zero.

If the simple exponential rate law is observed,

$$\tau = \frac{1}{\omega_o} ,$$

where ω_o is the frequency at which

$$\frac{\mathcal{R}(\omega)}{\mathcal{R}(0)} = \frac{1}{2} .$$

In practice, this simple rate law is usually not followed very closely, but the one-parameter concept is so convenient that it is retained as an approximation.

Responsivity is usually measured as a step in a detectivity determination for which a measurement of the narrow-band noise is also made. Narrow band is taken to mean $\Delta\omega \ll \omega$, and the noise voltage is customarily divided by $\Delta\omega^{1/2}$ to reduce to unit bandwidth. It is important that each section of the amplifier have a dynamic range sufficient to handle signals several times greater than the rms value of the noise for the bandwidth of that section, in order to avoid low readings caused by clipping. The signal and noise voltage measurements are usually accompanied by numerous cross-checks on instrumental noise, linearity, and gain calibration.

"Equal-energy" spectral response curves are ultimately ratio comparisons of the spectral response curves of the detector and a thermal detector of known departure from 100% absorptance. In making the comparison, a variety of chopped-beam

techniques is used, among them, separate spectral scans divided point-by-point; monochromator exit beam division in fixed ratio for the two detectors, followed by electronic ratio recording; and an exit beam division system in which the reference detector signal is held constant by servo-control of the monochromator slits. Insofar as the reference detector is a true power detector, the sample beam is then maintained at constant power. An improvement in signal-to-noise by a factor of two is obtained in systems where the sector chopper is made in the form of a front-surface optically flat mirror. Two optical paths are arranged so that the off-time for each detector is the on-time for the other.

NOL/Corona made a major improvement in the establishment of the reference response as recently as 1962 [1] when they enclosed a thermal detector in a miniature blackbody cavity and measured large departures from the 100% absorptance previously assumed for the most widely used thermal detectors.

6.2 Modified Detector Performance Tests

Some methods of modifying the standard tests for application to cross-correlation measurements have been considered, and they will now be described.

The employment of a digital computer as an intrinsic part of the crossed-beam correlator technique suggests that, for a linear signal channel, amplitude frequency response calibration over the 100 to 50,000 cps domain of interest may

be obtained appropriately in one or, at most, four observations by means of a square-wave modulated light source.

A square-wave chopper of the mirror type can be made to cut with sufficient sharpness to produce at least three odd harmonics at the theoretical 1/n amplitudes. Therefore, it is suggested that 10 seconds sampling time at each of perhaps 4 frequencies, 100, 500, 2,500, and 10,000 cps, be recorded, and that the power spectrum of the zero-delay value of the auto-correlation function be computed and displayed. A flat frequency response for the overall channel will be indicated by 1/n dependence of the height of the odd-harmonic peaks displayed. The great overlap of the sample spectra provides a check on the quality of the chopper square-wave form.

Simulation of a small modulation factor can be obtained by the superposition by means of a beam splitter of a small square-wave chopped intensity upon the unmodulated source employed in the correlation measurements. The modulation factor can be determined by chopping each beam and observing separately.

For correlation function measurements, it is assumed that the amplitude response, equalized to the optimum form as determined by means of the power spectrum of the flow phenomena under study, is somewhat modified to correct for differences in the phase transfer characteristics of the two detectors. More explicitly, a small sacrifice is made in flatness of the amplitude function in order to obtain equal phase at corresponding frequencies for the overall channels. One can verify this

condition by constructing the electrical difference of the two signals generated by square-wave modulated light beams of equal intensity and attenuating one signal to produce a null on an oscilloscope or rms voltmeter. Any residual signal at null is therefore caused by differential phase and amplitude inequality introduced by the detector-amplifier channels. If a null is not obtained, further diagnostic information may be obtained by passing the difference signal through a narrow band filter before oscilloscopic display or meter readout. Failure to obtain a null while observing an isolated frequency, preferably high for precision, indicates that the beams are not being chopped in phase. After this fault has been corrected by mechanical adjustment of the beam locations, the error signal may be re-examined at a lower harmonic, or lower fundamental. If a null cannot be obtained by readjustment of the gain, a phase mismatch at this frequency is indicated and can be corrected electronically. The adjustment is then repeated at several spot frequencies appropriate to the circuit.

If cutoffs at 100 and 50,000 cps are imposed, a procedure such as the above is required even with the employment of extremely fast, zero phase lag detectors, because the cut-offs imply the unavoidable introduction of large phase shifts near these frequencies. Since the cutoffs are introduced electronically by simple resistance-capacitance circuits of identical design, it is an easy matter to equalize the phase shift exactly over a range of frequencies by means of minor adjustments of circuit components.

PART II - SPECIFIC DETECTORS

1. PRELIMINARY SCREENING

Detectors were screened in four stages on the basis of speed of response, useful spectral range, realizable minimum relative random error, and relevant specialized features of specific models.

1.1 Speed of Response

Thermal detectors were eliminated from the survey because the fastest are 50-fold too slow for use up to 50,000 cps. This category includes vacuum thermocouples, bolometers, and the Golay detector.

The photoelectric detectors may be classified by mechanism of operation as photoemissive, photovoltaic, and photoconductive, with subclassification by alternative modes of operation such as photodiode and photoelectromagnetic operation. The photoconductive detectors may be subdivided into intrinsic and extrinsic types. In the former there are no energy levels in the forbidden band which may be occupied by electrons. The energy absorbed by the electrons from incident IR radiation must be sufficient to excite them to energy levels in the conduction band. In impurity or extrinsic semiconductors, there are impurity states in the forbidden band gap. Depending on the particular impurity which is introduced

during the crystal growing process, the incident IR radiation may cause electrons to be excited from the valency band to impurity on acceptor levels, as in n-type semiconductors, or electrons in donor levels in the forbidden band may be excited into the conduction band, as in p-type semiconductors.

Each of these types, however, shows advantages in restricted regions of the spectrum between 0.15 and 20 microns, and most of them are much faster than required. Therefore, no further categorical exclusions on the basis of mechanism were made.

The photoemissive mechanism is available with and without electron multiplication. Phototubes without multipliers are Nyquist-noise or amplifier-noise limited at low values of load resistance, and severely limited in frequency response at high values. However, all of the photocathodes that have not been superseded in quantum efficiency are available with secondary-emission multipliers built in to ease these limitations. Therefore, non-multiplier phototubes were categorically excluded. Gas-multiplication phototubes were excluded because they are not useful above 10,000 cps, and they also are rather nonlinear in contrast to their vacuum counterparts.

Some slow photoconductive detectors, such as lead sulfide and indium arsenide, are included because their detectivities are limited below 50,000 cps by a form of detector noise that, unlike the thermal detectors, decreases with frequency in the same ratio as the signal response. Equalization

during the crystal growing process, the incident IR radiation may cause electrons to be excited from the valency band to impurity or acceptor levels, as in n-type semiconductors, or electrons in donor levels in the forbidden band may be excited into the conduction band, as in p-type semiconductors.

Each of these types, however, shows advantages in restricted regions of the spectrum between 0.15 and 20 microns, and most of them are much faster than required. Therefore, no further categorical exclusions on the basis of mechanism were made.

The photoemissive mechanism is available with and without electron multiplication. Phototubes without multipliers are Nyquist-noise or amplifier-noise limited at low values of load resistance, and severely limited in frequency response at high values. However, all of the photocathodes that have not been superseded in quantum efficiency are available with secondary-emission multipliers built in to ease these limitations. Therefore, non-multiplier phototubes were categorically excluded. Gas-multiplication phototubes were excluded because they are not useful above 10,000 cps, and they also are rather nonlinear in contrast to their vacuum counterparts.

Some slow photoconductive detectors, such as lead sulfide and indium arsenide, are included because their detectivities are limited below 50,000 cps by a form of detector noise that, unlike the thermal detectors, decreases with frequency in the same ratio as the signal response. Equalization

is thus possible with no sacrifice in detectivity. Specific examples are given in Section 1.4.3.

1.2 Useful Spectral Range

1.2.1 Infrared

There is a general tendency for the detectivity to be lower for detectors of longer spectral cutoff wavelength. It may also be noted that long-wave spectral cutoff is determined almost entirely by gross chemical composition. Therefore, before further screening was made, detector types identified by chemical composition were arranged in order of increasing cutoff wavelength, $\lambda_{1/2}$. Because of the detectivity vs $\lambda_{1/2}$ relationship, competition in realizable signal/noise occurs within limited segments of this list.

For infrared detectors such compilations are available. Over a period of years, the Naval Ordnance Laboratory at Corona, California has conducted standardized performance measurements on several hundred developmental photodetectors under the Joint Services Infrared Sensitive Element Testing Program. The Corona reports, in general, include for each detector its measured frequency response, noise spectrum, and its detectivity as a function of frequency. The methods used in making these measurements are also given. These reports through April 1966 contain data on 21 types of detectors, of which 16 are infrared semiconductor quantum detectors, 3 are thermal detectors and, 2 are quantum detectors confined to the visible spectrum. Kruse, McGlauchlin and McQuistan [12] have

tabulated infrared detectors as of 1961 by chemical composition, with subclassifications by mode of operation (e.g., photoconductive, photovoltaic, or photoelectromagnetic) for those materials that usefully offer such options, and by detector temperature. Neither compilation includes infrared photomultipliers. With the inclusion of two multipliers, the 25 quantum types from the combined lists are collected in order of spectral wavelength cutoff in Table 1. An analogous list of UV and visible light detectors is given in Table 4. The detectivity - $\lambda_{1/2}$ trend may be seen. This trend, together with a general tendency to show maximum detectivity near the cutoff, indicates the desirability of employment of several detectors to cover the range from 1 to 20 microns. At wavelengths less than 1 micron, photomultipliers are seen to have an overwhelming advantage in detectivity. However, it will be shown in Section 1.3 that in the general case detectivity cannot be used without qualification as a reciprocal measure of random relative error in radiation signal measurements.

Table 1 Infrared Detector Types

Type	Cutoff Wavelength+ Microns	D* Peak++ $cm \cdot cps^{1/2} watt^{-1}$	τ μsec	T °K
*S-20 photocathode	0.62	4×10^{17}	< 0.01	196
selenium oxide	.69	1.2×10^{11}	910	295
cadmium selenide	.72	2.1×10^{11}	12000	295
gallium arsenide	.89	4.5×10^{11}	1000	295
*S-1 photocathode	.96	8×10^{15}	< 0.01	196
*silicon	1.0	2×10^{12}	< 1	297
thallous sulfide	1.1	2.2×10^{12}	530	295
germanium-silicon alloy	1.1-1.85			
germanium	1.85			
germanium:gold, antimony	2.	2.5×10^{10}	110	77
*lead sulfide	2.5-3.3	4×10^{11}	200	195
*indium arsenide	2.5-3.4	5.4×10^{11}	-	77
tellurium	3.8	6×10^{10}	60	77
lead telluride	4.0	2.7×10^{9}	25	77
lead selenide	3.4-4.5	1.1×10^{10}	48	77
mercury cadmium telluride	6.5	1.5×10^{7}		298
*indium antimonide	5.5-7.0	6×10^{10}	< 2	77
*germanium: gold	7.0	4×10^{10}	< 1	65
germanium-silicon:gold	10.1	7×10^{9}	0.1	50
germanium-silicon:zinc, antimony	13.3	1.0×10^{10}	0.1	50
*germanium:mercury	13.5-14	1.1×10^{10}	< 1	4
germanium:zinc, antimony	15.	3×10^{9}	-	50
*germanium:cadmium	21.5	1.8×10^{10}	-	< 25
*germanium:copper	27	2.5×10^{10}	-	< 20
germanium:zinc(ZIP)	39.5	1.0×10^{10}	< 0.01	4.2

+ Wavelength at which equal-energy spectral response is 50% of peak.

++ D* defined in text.

* Relevant

A few entries in Table 1 may be eliminated on various grounds; the detectors remaining for more detailed consideration have been starred.

Lead selenide (long wavelength cutoff 4.5) and lead telluride (4.0μ) are chemical analogues of lead sulfide; they were developed with the objective of extending coverage to the 3-5μ region, of military interest because it is a long-path atmospheric window. Interest in these materials dwindled with the discovery of the spectacularly high charge carrier mobility of indium antimonide. Levinstein,[13] who played a leading role in the development of lead telluride detectors, said recently, "it did not lend itself to production techniques and is no longer available." Lead selenide is now of interest primarily where room temperature operation is desirable, not a consideration in the crossed-beam application. The remaining unstarred intrinsic detectors are of low detectivity.

The germanium and germanium-silicon detectors are extrinsic types. Some of them were tailored to exploit the second long-path atmospheric window, 8.5-13 microns, for military applications. The germanium:zinc detector was eliminated because its special attribute is the extension of spectral range from 27 to 40 microns, a region outside of our concern.

1.2.2 Ultraviolet and Visible

The spectral response characteristics of detectors for the UV, visible, and near infrared are usually designated by S-numbers, which are defined, to date, by

24 standard curves set up by agreement among manufacturers through the Electronic Industries Association. Small variations from these standard curves for different manufacturers will be ignored in this survey. The S-number designation, however, includes effects of window transmittance and multiple reflections on quantum efficiency, and thus there are more types and fewer actual materials than designations. One anticipates that this general classification does not describe all detectors satisfactorily, and, indeed, exceptions are made by manufacturers. The RCA 7046 photomultiplier, for example, is qualified as having an "extended S-11 response", the extension being into the UV. The RCA 931-A, 4471 and 4472 photomultipliers are all designated as S-4 types and are identical except that the latter have controlled sensitivities above 5800A for applications where red/blue sensitivity ratio is important. Electro-Mechanical Research, Inc., do not employ the S-number code, although they classify by chemical material; they provide a spectral curve for each model number. The 24 types are listed in Table 2, taken from the RCA technical manual. Spectral response curves for most of these are given in Figs. 4 and 5, as presented by RCA and ITT Industrial Laboratories, Fort Wayne, Indiana, respectively.

Important UV window materials in use but not included in the E.I.A. classification are lithium fluoride and selected UV grades of sapphire (aluminum oxide). Short-wavelength cutoffs for these windows are given in Table 3.

TABLE 2

TYPICAL COMBINATIONS OF PHOTOSENSITIVE SURFACES AND WINDOW MATERIALS WHICH CAN PROVIDE THE BASIC SPECTRAO-RESPONSE DESIGNATIONS STANDARDIZED BY E.I.A.

Spectral Response Number	Type of Photodetector	Photosensitive Material	Envelope
S-1, S-2*	Photocathode	Ag-O-Cs	Lime-glass
S-3	Photocathode	Ag-O-Rb	Lime-glass
S-4	Photocathode	Cs-Sb	Lime-glass
S-5	Photocathode	Cs-Sb	UV-transmitting glass
S-6	Photocathode	Na	Unspecified
S-7	Photocathode	Cs-Rb-O-Ag	Pyrex
S-8	Photocathode	Cs-Bi	Lime-glass
S-9	Photocathode	Cs-Sb(semitransparent)	Lime-glass
S-10	Photocathode	Ag-Bi-O-Cs (semitransparent)	Lime-glass
S-11	Photocathode	Cs-Sb(Semitransparent)	Lime-glass
S-12	Photoconductor	CdS(crystal with plastic coating)	Lime-glass
S-13	Photocathode	Cs-Sb(semitransparent)	Fused silica
S-14	Photojunction (Photocell)	Ge	Lime-glass
S-15	Photoconductor (Photocell)	CdS (sintered)	Lime-glass
S-16	Photoconductor (Photocell)	CdSe	Lime-glass
S-17	Photocathode	Cs-Sb (reflecting substrate)	Lime-glass
S-18	Photoconductor (Vidicon)	Sb2Se	Lime
S-19	Photocathode	Cs-Sb	Fused silica
S-20	Photocathode	Sb-K-Na-Cs (semitransparent)	Lime-glass
S-21	Photocathode	Cs-Sb(semitransparent)	UV-transmitting glass
S-22	Presently Unspecified		
S-23	Photocathode	Rb-Te	Fused silica
S-24	Photocathode	Na_2KSb	Lime-glass

*Now obsolete. Formerly a variation similar to S-1, discarded by EIA action to reduce confusion.

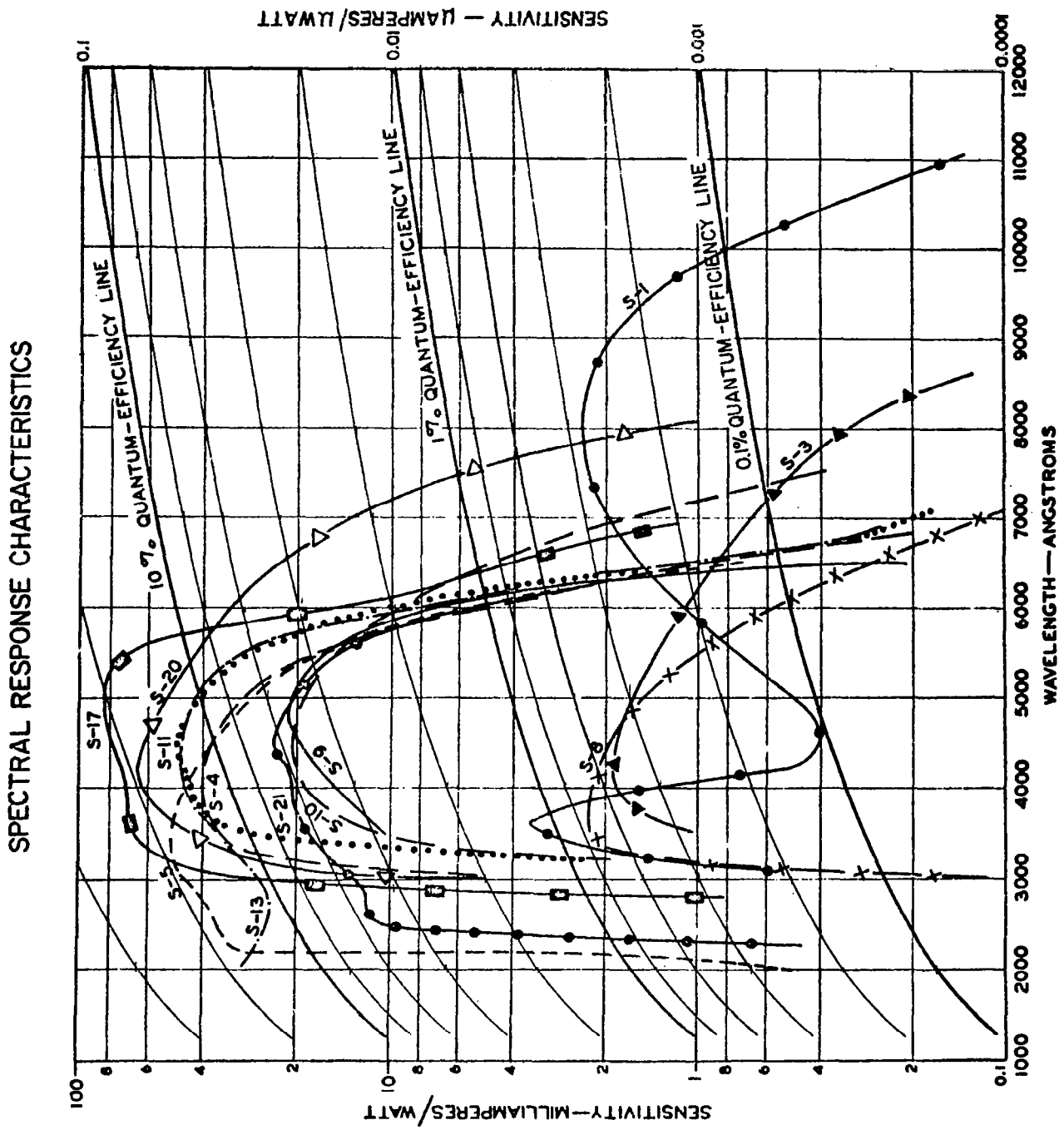

Fig. 4 Photocathode Spectral Response Characteristics (ITT)

RELATIVE SPECTRAL RESPONSE CHARACTERISTICS

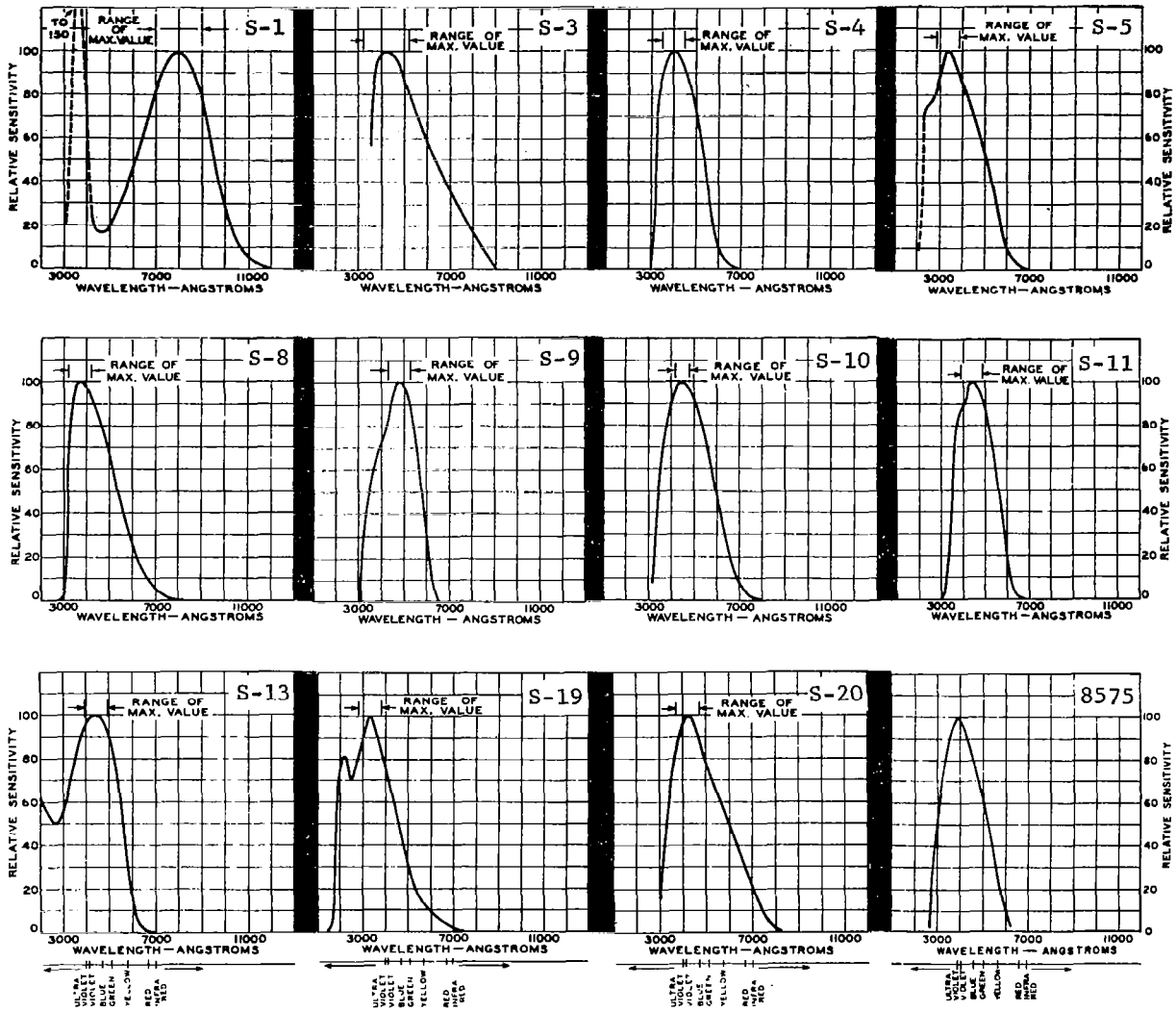

Fig. 5 Relative Spectral Response Characteristics (RCA)

Table 3

Ultraviolet Window Materials

Material	Short-wave cutoff, (microns) for transmittance of 50%	1%
Lithium fluoride, 5 mm	0.110	0.105
Magnesium fluoride, 5 mm		~0.115
Sapphire, 1 mm	0.153	0.145
Corning 9741 vitreous silica, 1 mm	0.34	0.22
Corning 7056 borosilicate glass	-	0.32

Six additional UV cathode materials not included in Table 2 are available with the above windows in all appropriate combinations.

All cathode types available in photomultiplier tubes including variants resulting from reflective backings are included in Table 4.

Some of the detector types of Table 4 can be excluded on the basis of low quantum efficiency. The first six entries are "solar blind" cathodes whose advantages are low dark current and ability to monitor UV lines such as Lyman-alpha in the presence of a high background intensity of solar radiation. Low dark current means high detectivity, but in Section 1.3 it is shown that, for detectivities greater than 1.6×10^{12} $cps^{1/2}/watt$, $(QE)^{1/2}$ rather than detectivity is the inverse measure of relative random error. Toward the end of the list, detectivities approach this limit, and one photoconductive detector, the silicon photodiode, competes in the near infrared with the S-1 photomultiplier. The S-1 photocathode has an unusually low quantum efficiency, but it has no other competitor at wavelengths longer than 0.9 microns. Cadmium sulfide and selenide vary in responsivity with previous light exposure.

For typical examples of the detector types selected from Tables 1 and 4 for further consideration, nominal specific signal/noise ratios, $D_{\Delta f}$, (rms signal/rms noise per rms watt of modulated light) were calculated from the D* values of unusually small-area detectors for the particular conditions Δf = 100 to 50,000 cps and detector area $A = 2.5 \times 10^{-3} cm^2$, from the equations

$$D_{\Delta f} = 11.18\ D^*$$

where $$(A\Delta f)^{1/2} = 11.18\ cm \cdot cps^{1/2}$$

Table 4

Ultraviolet and Visible Light Detector Types

Type	EIA Code	$\lambda_{1/2}$ † microns	$\lambda_{.001}$ ‡ microns	QE_{peak} %
KBr	None	.134	.16	20
CsBr	None	.145	.18	20
RbI	None	.149	.19	20
CsI	None	.151	.20	8-20
CuI	None	.165	.20	3
CsTe	None	.26	.35	7
SbNaK	S-24	.50	.72	24
SbCs	S-4	.54	.66	12
SbCs	S-11	.56	.66	14
*SbCs	S-11	.56	.66	17
*SbCs	S-13	.56	.66	14
*SbCs	S-17	.56	.7	24
AgBiOCs	S-10	.59	.74	6
*SbKNaCs	S-20	.60	.83	20
*SbKNaCs	S-20 refl.	.60	.85	30
AgORb	S-3	.63	.72	0.58
CdS	S-15	.66	-	50
CdSe	S-16	.72	-	50
*AgOCs	S-1	.97	1.0	0.4
*Si	None	1.0	1.2	70
Ge	S-14	1.7	-	30

*Relevant

‡ $\lambda_{.001}$: Wavelength for 0.1% quantum efficiency

† $\lambda_{1/2}$: Wavelength for power response 50% of peak power response.

This small area (0.5 x 0.5 mm) is appropriate for a 3mm diameter, or smaller, spectrometer exit aperture followed by a 6:1 demagnification. An elliposidal mirror of such ratio is routinely employed in instruments of focal ratios in the order of f/5 to f/11. The wide-band detectivities $D_{\Delta f}$ are listed in Table 5.

Table 5

Typical Peak Spectral Wide-Band Detectivities

for 1/2 x 1/2 mm Detectors

Type	EIA Code	T °K	QE_{peak} %	D* cm $cps^{1/2}{}_w$-1	$D_{\Delta f_w}$-1
SbCs	S-11	300	14	-	-
SbCs	S-13	300	14	-	-
SbKNaCs	S-20	196	20	-	-
SbKNaCS	S-20	300	30	-	-
AgOCs	S-1	300	0.4	-	-
AgOCs	S-1	196	0.4	$8x10^{15}$	$7x10^{14}$
silicon		300	70	$1.8x10^{12}$	$1.6x10^{11}$
lead sulfide		195	<50	$4x10^{11}$	$3.6x10^{10}$
indium arsenide		77	<100	$5.4x10^{10}$	$4.8x10^{9}$
indium antimonide		77	<100	$6x10^{10}$	$5.4x10^{9}$
germanium:gold		65	<50	$4x10^{10}$	$3.6x10^{9}$
germanium:mercury		4	<50	$1.1x10^{10}$	$1.0x10^{9}$
germanium:cadmium		<25	<35	$1.8x10^{10}$	$1.6x10^{9}$
germanium:copper		<20	<35	$2.5x10^{10}$	$2.2x10^{9}$

A single number, however, is an inadequate basis for comparison of detectors, because the criterion of choice for maximum precision of measurement of correlation functions depends on the mean intensity incident on the detector. This intensity depends on the choice of light source and, hence, is an unspecified variable. This intensity, therefore, has been made the independent variable in graphical and algebraic representations of precision in the following sections of this report. The relationship between precision and detectivity is discussed in the next section.

1.3 Relative Precision and Signal/Noise Ratio

1.3.1 Extension of the Signal/Noise Ratio Concept

Detectivity is a specific signal/noise ratio per rms watt of optical input, measured in a 1 cps bandwidth. It is the principal performance parameter measured by detector manufacturers because, with qualifications, signal/noise ratio is a reciprocal measure of the relative random error to be expected in the comparative measurements of modulated light intensities. The qualifications are that the noise is tacitly assumed to be independent of the optical signal, that the signal is proportional to the rms input, that $S/N \gg 1$, and that S is periodic. For ultraviolet and visible light measurements, the first assumption is usually false; for large mean intensities, the second is sometimes false, and for cross-correlation turbulence measurements, the third and fourth assumptions are always false. The signal/noise ratio concept must be

sufficiently generalized to apply to these circumstances.

The customary detectivity evaluation consists of two parts, a responsivity measurement and a noise measurement. A radiation source of known mean power unit area, $\overline{\Phi}/A$, at the detector is modulated periodically by means of a rotating chopper of known modulation wave form m(t). The rms value S of the fundamental component of the signal voltage s(t) appearing at the output of the detector circuit is measured by means of a narrow band amplifier of bandwidth Δf_1 centered on the fundamental chopper frequency, followed by a square-law AC voltmeter. In more strict terms the quantity measured is V, the quadratic sum of signal and noise present in the bandwidth Δf_1:

$$V^2 = S^2 + N^2$$

The mean intensity employed, however, is made sufficiently high that $S^2 \gg N^2$ and $V^2 \sim S^2$.

An rms noise reading is then made in the same bandwidth by cutting off the source stimulus. This cutoff may be made in two ways. Usually a shutter is closed or the chopper is stopped in the off-position, resulting in a measurement N_d. Alternatively, the chopper can be stopped in such a position that the incident unmodulated intensity is $\overline{\Phi}$. The measured noise N_2 then includes the signal shot noise N_{ss}.

$$N^2 = N_d{}^2 + N_{ss}{}^2$$

Responsivity $\mathcal{R}$, detectivity D, noise-equivalent power NEP (equivalent noise input NEI), $D_{\Delta f}$ and D* are defined by the following equations:

$$\Phi = M\bar{\Phi} \quad \text{rms watts} \tag{1}$$

$$S = \mathcal{R}\Phi \quad \text{rms volts} \tag{2}$$

$$D_{\Delta f} = \mathcal{R}/N_d \quad \text{rms watts}^{-1} \tag{3}$$

$$D = D_{\Delta f}\ \Delta f^{1/2}\ \text{cps}^{1/2} \cdot \text{rms watt}^{-1} \tag{4}$$

$$D^* = DA^{1/2}\ \text{cm}\cdot\text{cps}^{1/2} \cdot \text{rms watt}^{-1} \tag{5}$$

$$NEP = 1/D \quad \text{rms watts} \cdot \text{cps}^{-1/2} \tag{6}$$

$$SEN = 1/D_{\Delta f} \quad \text{rms watts} \tag{7}$$

where M is the rms value of m(t) and $\bar{\Phi}$ is in watts. For square-wave chopping $M = 2\sqrt{2}/\pi$ and peak intensity is $2\bar{\Phi}$. The symbol SEN (signal-equivalent of noise) has been introduced here as a noise-equivalent power for the bandwidth Δf, in order to avoid confusion with the well-established unit-bandwidth symbol NEP. $\mathcal{R}$ may be eliminated from equations (2) and (3) to show the tacit proportionality underlying the definitions:

$$\frac{S}{N} = \frac{\Phi}{SEN} \cdot$$

From the equation $V^2 = S^2+N^2$, it may be seen that for S/N = 10, a systematic error of +1% is made in taking the voltmeter deflection V^2 to represent S^2, and an error of +1/2% in taking the voltmeter reading V to be S. In addition

to exhibiting a small systematic error, the deflection fluctuates, and the relative random error, defined as the relative standard deviation in the departure of $V^2(T)$ from V^2, is inversely proportional to S/N for $S/N \gg 1$, S sinusoidal, N narrow-band.

If S is random, and $S/N \gg 1$, the standard deviation is proportional to S^2 and independent of N; therefore the relative standard deviation is independent of S/N.

For cross-correlation detection of random signals, in contrast to square-law detection of periodic or random signals, it is no longer necessary that $S \gg N$. In this more general case, which includes square-law detection at $S \gg N$ as a special case, the relationship between S/N and relative standard deviation is neither an inverse proportionality nor a constant. The general case is given for $\beta \gg 1$ by the equations[14]

$$R(\tau) = S^2 e^{-\alpha}$$

$$\frac{S^2}{\sigma} = \frac{\beta^{1/2}}{\left[k + \left(\frac{N_1}{S}\right)^2 + \left(\frac{N_2}{S}\right)^2 + \left(\frac{N_1}{S}\right)^2 \left(\frac{N_2}{S}\right)^2\right]^{1/2}} \qquad (8)$$

where $R(\tau)$ = correlation function (the output)

σ = standard deviation in R or S^2

τ = delay time

$\alpha = \pi\Delta f\tau$

$\beta = \pi\Delta fT$

T = integration time

N_1, N_2 = total noise in the respective channels including signal shot noise and uncorrelated turbulence N_u

k = a monotonic function of α

such that k = 2 when $\alpha = 0$ and k = 1 when $0 \ll \alpha < \beta$.

For large and equal noise in both channels, i.e., $N_1 = N_2 = N$ and $S/N \ll 1$, only the last term of the denominator remains, and

$$\frac{S^2}{\sigma} = \beta^{1/2} \left(\frac{S}{N}\right)^2 . \tag{9}$$

In this case, then $(S/N)^2$ may be taken as a proportionate measure of the relative precision in measurement of S^2.

In contrast, for the special case of a random signal into a square-law detector at $S/N \gg 1$, one has $N_1 = N_2 = N$ and k = 2, and

$$\frac{S^2}{\sigma} = \left(\frac{\beta}{2}\right)^{1/2} , \tag{10}$$

which is independent of S/N, as stated. Equation (8) is not sufficiently general, however, to describe the error for periodic signals.

For crossed-beam applications, it would be convenient to be able to use the simple approximation of equation (9) rather than equation (8), but substitution of realistic data shows the resulting error to be appreciable. For example, there were 6 eddies across one experimental jet, and hence $(N/S)^2 = 5$. The error in computing S^2/σ from equation (9) instead of equation (8) is 22%. At 11 eddies, $(N/S)^2 = 10$, and the corresponding error is 11%. At $N/S > 1$, most of this error is caused by the omission of the contribution to σ of the nonperiodic fluctuation s(t) itself.

A minimum useful S/N may be calculated from equation (8). If the maximum permissible relative error in a correlation function measurement is taken to be 10% of the maximum value and maximum practical integration time as 10 sec., substitution of $S^2/\sigma = 10$ and $T = 10$ results in $S/N_{min} = 0.089$.

In summary, if S/N ratio is to be regarded as a measure of relative precision in measurement of S^2 or $R_{max.}$, it must be taken as a nonlinear measure given by eq. (8), approximately quadratic for $S/N < 0.3$, and N must be the total noise including signal shot noise and uncorrelated turbulence, as well as detector and background noise. Equation (8) applies only to random signals.

1.3.2 Graphical Description

The purpose of this section is to show at what absolute mean intensities incident on the detector the various components of N^2 predominate. Rather than noise vs. intensity, as an indirect measure of absolute error, signal/noise ratio vs. intensity was plotted as an indirect measure of relative error. In using the graphs, mean intensities are calculated for a particular pair of sources, and S/N ratios read from the graph. The S/N ratios are then substituted into equation (8) to obtain relative error in measurement of S^2. In order to reduce the number of independent variables, the curves were drawn for a set of arbitrarily fixed conditions: the rms correlated signal fluctuation was assumed to be 1% of the mean intensity, and there were assumed to be 11 eddies across the flow. In symbols, $M = 0.01$ and $M_u^2/M^2 = 10$. Input bandwidth Δf was taken as 50,000 cps. Each curve was drawn for a selected wavelength appropriate for comparison.

Figure 6 is a sample graph describing the signal/noise ratio of a lead sulfide detector at 3 microns wavelength. The curves were drawn to illustrate the following kinds of information:

(1) This detector is detector-noise limited below 1.8×10^{-9} mean incident watts, and turbulence-noise limited above this value for the assumed conditions,

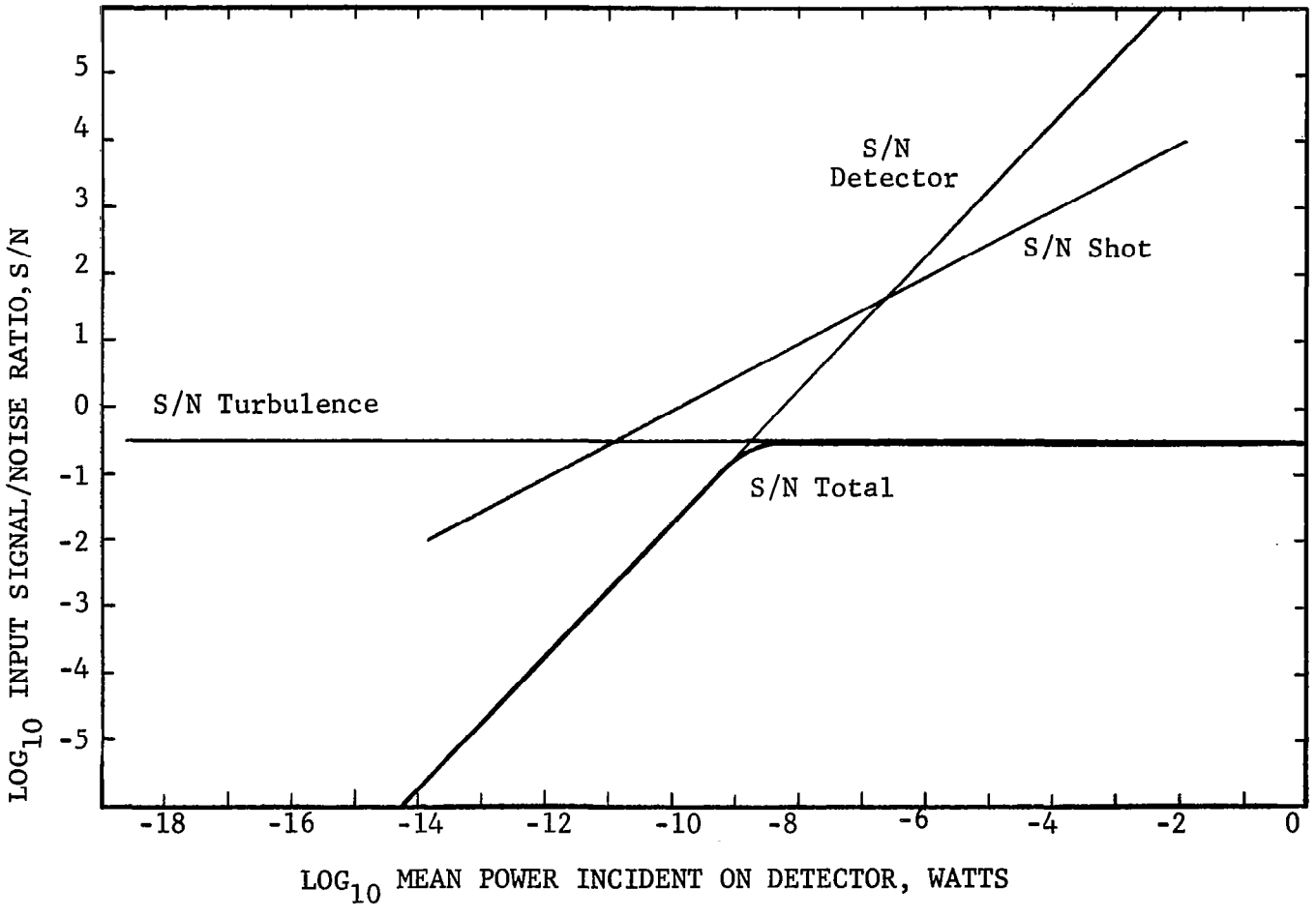

Fig. 6 Dominant Noise Terms in a Lead Sulfide Photoconductor

(2) There is no mean incident intensity at which this detector becomes signal-shot-noise limited for these assumed conditions,

(3) If, however, M were 10^{-5} rather than 10^{-2}, with 10 eddies across the flow, the detector would be signal shot noise limited between 2.4×10^{-7} and 1.2×10^{-5} watts,

(4) No further advantage is gained in S/N and hence in R/σ above 1.8×10^{-9} watts at $M_u = 3.16\%$,

(5) For an integration time of 10 sec., the minimum useful mean intensity for this detector is 5.0×10^{-10} watts, if the minimum use R_{max}/σ is taken as 10.

How these conclusions are read from the graph will now be described.

The components S/N_{ss}, S/N_d, and S/N_u are shown in the log-log plot as three straight lines of slopes 1/2, 1, and 0, respectively, representing the power dependencies on $\overline{\Phi}$. The equations for these curves are

$$S/N_{ss} = \left[\frac{M^2 \lambda (QE)}{hc2\Delta f}\,\overline{\Phi}\right]^{1/2} \tag{11}$$

$$S/N_d = D_{\Delta f} M\,\overline{\Phi} \tag{12}$$

$$S/N_u = M/M_u = 10^{-1/2} \tag{13}$$

where $M = 0.01$

$M_u = 0.0316$

$\lambda = 3$ microns

$QE = 0.50$

$\Delta f = 5 \times 10^4$ cps

$hc = 1.986 \times 10^{-19}$ micron·joules/photon

$D_{\Delta f} = 1.8 \times 10^{10}$ watts^{-1}

The mean powers at intersections of these curves, indicated by the corresponding subscripts, may be computed by the following equations:

$$\overline{\Phi}_{ssd} = \frac{\lambda(QE)(NEP)^2}{2hc} \tag{14}$$

$$\overline{\Phi}_{du} = (SEN)/M_u \tag{15}$$

$$\overline{\Phi}_{ssn} = \frac{hc2\Delta f}{\lambda(QE)M_u^2} \tag{16}$$

The curve representing S/N is drawn bold-face. Since there is no point at which all three components are of comparable magnitude, the log S/N function is composed of nearly linear regions asymptotic to the component of smallest algebraic value in each region. The transitional portions have inflections at points 1.5 mm below the intersection of the asymptotes for the one cycle/cm log scale employed. On this scale 1.5 mm represents

a factor of $\sqrt{2}$. At the abscissa of intersection, the two relevant mean square noise powers are equal. Thus, at $\bar{\Phi} = 1.8 \times 10^{-9}$ watts,

$$N^2 = N_d^2 + N_u^2 + N_{ss}^2$$

$$= N_d^2 + N_u^2, \text{ approx.}$$

$$= 2N_d^2$$

$$N = \sqrt{2}N_d.$$

Since the shot noise curve lies 10 mm above this intersection, an error of only 0.5% is made in ignoring the N_{ss}^2 term. Since there is no mean intensity at which S/N_{ss} is the lowest curve of the three, there is no mean intensity at which the detector is signal shot noise limited. However, if M_u and M were reduced 1000-fold, the S/N_{ss} and S/N_d curves would be displaced downward 1000-fold (3 cm) and a segment of the S/N_{ss} curve would be included above the intersection of S/N_{ss} and S/N_d at $\Phi_{ssd} = 2.4 \times 10^{-7}$ watts. Thus, in the absence of turbulence, shot noise would predominate above this intensity, detector noise below it. Above 1000 $\bar{\Phi}_{ssu}$, turbulence would once again predominate.

For the minimum useful S/N = 0.089 previously suggested, the corresponding $\overline{\Phi}_{min}$ for the lead sulfide detector = 5×10^{-10} watts. A detective quantum efficiency (QE) of 50% was assumed for reasons given in Section 4.2.

Figure 7 shows an S-1 multiplier at 0.8 microns for two temperatures. At either 300°K or 196°K the signal/dark current shot noise ratio is large in comparison to S/N_d of the lead sulfide detector. The detector noise at 300°K is less than the signal shot noise for $\overline{\Phi}$ greater than 6×10^{-12} watts. Since, for this photomultiplier, the detector noise is entirely dark current shot noise and, since the mean cathode current is linear with mean intensity, this cross-over is merely the mean intensity at which the D.C. photocurrent equals the D.C. dark current, and equation (14) is scarcely required for the evaluation. However, equation (14) is based on the more fundamental point that it is the equality of the rms noise terms that defines the intersection, and equality of D.C. and differential responsivities need not be assumed. Precursor equation (11) is an operational definition of detective quantum efficiency.

Figure 7 also shows that, with $\overline{\Phi}$ above the useful minimum (5.6×10^{-10} watts) for 10 sec. integration time, this S-1 detector is signal-shot noise limited at 300°K, and therefore cooling is unnecessary.

The effect of an increase in quantum efficiency by some factor is to displace the S/N_{ss} curve to the left by that factor or, what amounts to the same thing, upward by the

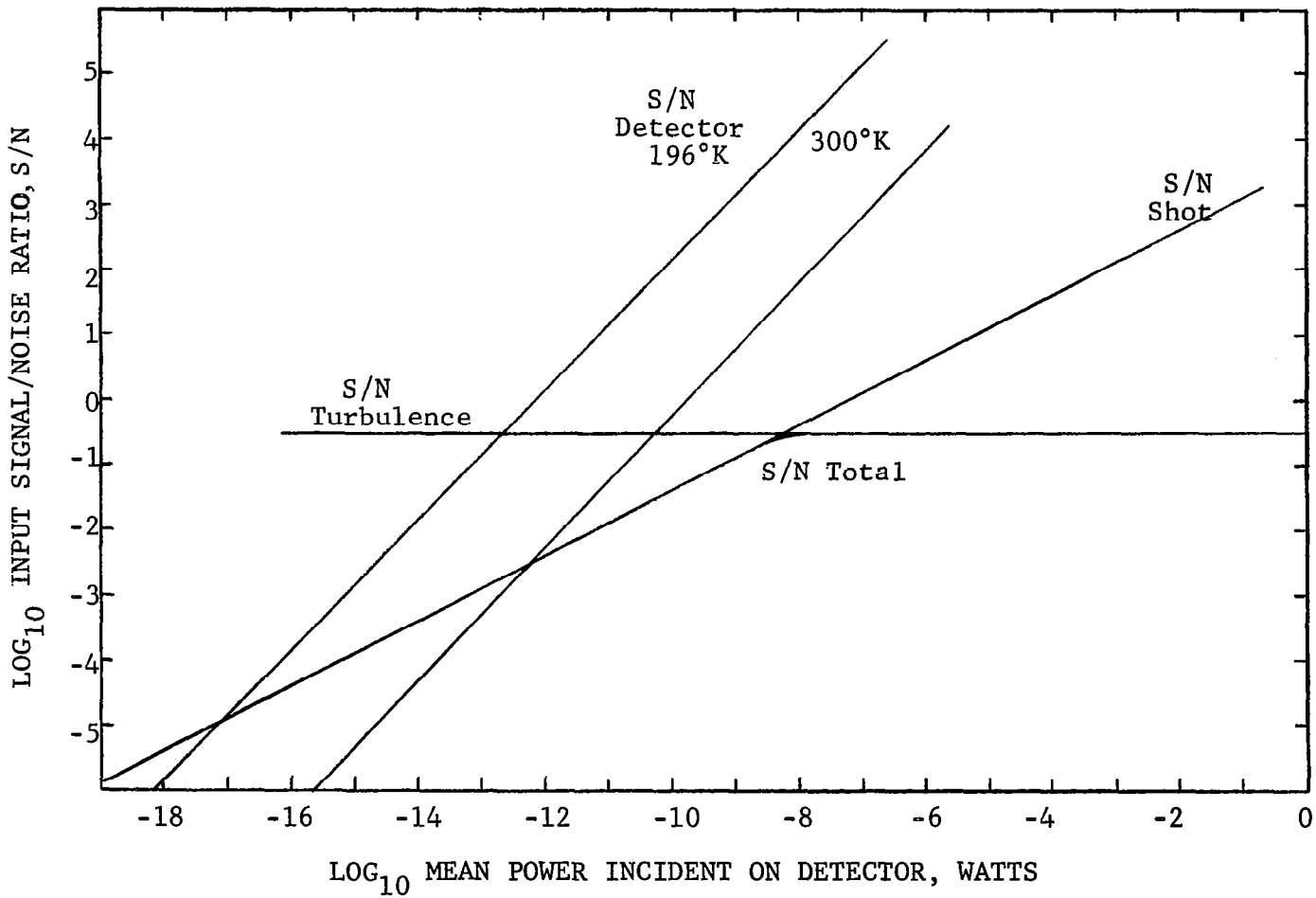

Fig. 7 Dominant Noise Terms in an S-1 Photomultiplier

square root of that factor. Thus, at a given S/N_{ss}, the minimum usable $\overline{\Phi}$ varies inversely with the quantum efficiency, and at a given $\overline{\Phi}$, the S/N_{ss} improves as the square-root of the quantum efficiency.

1.4 Comparative Signal/Noise Ratios

The relevant spectrum seems to divide naturally into four regions, a short-wavelength region of high photoelectric quantum efficiency, a transitional region in the red and near infrared, an intrinsic photoconductor region, and an extrinsic photoconductor region dominated by doped germanium crystals. Tabulations were made of specific makes and models of the entries of Table 5 and grouped for discussion in accordance with the four regions. However, significant cross-over mean intensities as defined in Section 1.3.2 have been collected in Table 6 from all sections. Abbreviations used for the manufacturers listed in Tables 7 through 10 are as follows:

AMP	Amperex	PM tubes
AVCO	Avco Corp., Electronics Div.	InSb
DUM	DuMont Labs.	PM tubes
EGG	Edgerton, Germeshausen and Grier	Si
EK	Eastman Kodak	PbS, PbSe

EMI	Whittaker Corp., Gencom Div.	PM tubes
EMR	Electromechanical Research	PM tubes
ENL	Electronuclear Labs.	Si, InSb, InAs, Ge
ITT	ITT Industrial Labs.	PM tubes
RAY	Raytheon	Ge:Au, Ge:Hg, Ge:Cd, Ge:Cu
RCA	Radio Corp. of America	PM tubes
SBRC	Santa Barbara Research Center	PbS, PbSe, InAs, InSb, Ge:Au, Ge:Hg, Ge:Cu
TXI	Texas Instruments	Si, InAs, InSb, Ge:Hg, Ge:Cu
UDT	United Detector Technology	Si

Table 6a

Make and Model of Detectors Illustrated in Graphs

Fig.	Type & Mode		Make & Model*	$A^{1/2}$ cm	T °K	NEP** watts/$cps^{1/2}$	SEN** watts	QE %
6	PbS	PC	SBRC - 180°FOV	.05	77	2.5-13	5.6-11	<50
7	S-1	PM	ITT FW-143	.225	300	9.1-13	2.0-10	.4
	S-1	PM		.225	196	3.2-17	7.3-15	.4
8	S-11	PM	ITT FW-136	.225	300	1.3-15	2.9-13	14
	S-20	PM	ITT FW-143	.225	300	1.1-15	2.5-13	20
	Si	PD	EGG SGD-100	.225	300	4.0-12	8.9-10	14
10	S-20	PM		.225	300	3.2-15	7.2-13	4.3
	Si	PD		.225	300	9.9-13	2.2-10	56
11	S-1	PM		.225	196	3.2-17	7.3-15	.4
	Si	PD		.225	300	8.4-13	1.9-10	66
12	PbS	PC		.05	77	2.5-13	5.6-11	<50
	InSb	PV	TXI ISVA 50°FOV	.05	77	5.4-13	1.2-10	<100
	InAs	PV	TXI IAV 180°FOV	.05	77	2.5-13	5.6-11	<100
13	PbS	PC		.05	77	2.3-13	5.0-11	<50
	InSb	PV		.05	77	4.2-13	9.8-11	<100
	InAs	PV		.05	300	1.8-11	4.2-9	<100
14	InSb	PV		.05	77	2.9-13	6.4-11	<100
14	Ge:Cu	PC	RAY QKN 1009-90°	.044	4.2	2.1-12	4.7-10	<50

* A blank indicates same make and model as previous entry of that type.

**To simplify tabulation, exponential notation in Tables 6 through 8 has condensed so that 2.5-13 means 2.5×10^{-13}, etc.

Table 6b

Signal/Noise - Crossover Mean Intensities, Watts

Fig.	Type	T °K	$\overline{\Phi}_{ssd}$	$\overline{\Phi}_{du}$	$\overline{\Phi}_{ssu}$	$\overline{\Phi}_{min}$	$\overline{\Phi}_{x}$
6	PbS	77	2.5-7	2.0-11	1.5-11	5.0-10	
7	S-1	300	6.5-9	6.5-11	6.0-9	5.0-10	
	S-1	196	8.5-18	2.5-15	6.0-9	5.0-10	
8	S-11	300	2.5-13	9.0-14	3.5-10	2.8-11	2.0-6
	S-20	300	2.5-13	8.0-14	2.5-10	2.0-11	3.0-6
	Si	300	2.0-6	3.0-10	3.5-10	8.0-9	
10	S-20	300	7.0-13	2.0-13	7.0-10	5.5-11	7.0-8
	Si	300	9.0-7	7.0-11	5.5-11	2.0-9	
11	S-1	196	8.5-18	2.5-15	6.0-9	5.0-10	5.5-9
	Si	300	9.5-7	6.0-11	4.0-11	1.5-9	
12	PbS	77	2.5-7	2.0-11	1.5-11	5.0-10	
	InSb	77	2.0-6	4.0-11	6.5-12	1.0-9	
	InAs	77	4.5-7	2.0-11	6.5-12	5.0-10	
13	PbS	77	2.5-7	1.5-11	1.0-11	4.5-10	
	InSb	77	1.5-6	3.0-11	5.0-12	8.5-10	
	InAs	300	3.0-7	1.5-9	5.0-12	3.5-10	
14	InSb	77	5.5-6	2.0-11	3.5-12	5.5-10	
14	Ge:Cu	4.2	9.0-7	1.5-10	2.5-12	4.0-9	

1.4.1 0.15 to 0.55 Microns

Specific detector makes and models for this range are given in Table 7. In this region the most efficient photomultipliers (S-11 and S-20) are signal-shot-noise limited above 5×10^{-13} watts which is so low that, with the usual assumed M and M_u, they would require 10^5 seconds integration time for useful data. These detectors and a silicon photodiode are depicted in Fig. 8 at 0.4 microns wavelength. The multipliers are turbulence limited before the diode has reached the useful minimum. Above 3.5×10^{-7} watts the diode is also turbulence limited for the assumed 1% correlated turbulence and 3.2% uncorrelated turbulence.

For low-noise photomultipliers, for a radiant energy input greater than 5×10^{-13} watts, the S/N ratio is proportional to the square root of quantum efficiency. Therefore, large numbers of special-purpose photomultipliers designed for remarkably low dark current and noise equivalent power may be dismissed. Improvement of quantum efficiency, however, is another active area of development. Increases from the standard 14 to 20% level to greater than 30% are in the development stage. Figure 9 shows the spectral response of some high-quantum efficiency variants of the S-20 multialkali response characteristic. Current state-of-the-art for an opaque multialkali cathode on a reflecting substrate is shown for the RCA developmental C70038D (10 stages) and the EMR 641E-01-18 (18 stages). The EMR curve has been extended to show the effect of a hypothetical lithium

Table 7a
Short Wavelength Photomultipliers
SbCs

Type	Make, Model,	Stages	d., mm	QE_{pk} %	λ_{pk} μ	$\lambda_{1/2}$ μ	NEP at 300°K watts/cps$^{1/2}$	Remarks
S-11					.42	.55		
AMP	XP1115	10	14	18			2.0-15	
AMP	XP1113	6	14	10			5.1-15	Ruggedized
AMP	XP1114	4	14	10			1.6-14	10^{-4} watts max.
DUM	K1303	6	13	13			-	Ruggedized
EMI	6094B	11	10	17			7.5-17	
EMR	541A-01-14	14	25	15	.41		4.0-16	Potted
ITT	FW-136	16	2.5	14	.44		1.3-15	Ruggedized
RCA	7767	10	13.	14			4-15	
RCA	7764	6	13.	16			3-14	
S-13					.42	.55		
AMP	XP1118	10	14	18			2-15	
DUM	K1566	10	13	13			-	Potting avail.
EMI	6256B	13	10	17			1.1-16	
EMR	541A-05-14	14	15	14	.41		3.7-16	Potted
Non-std								
EMI	6256S	13	10	13	.42	.55	5.7-17	
EMR	641A-03-18	18	10	23	.41		4.6-16	Potted, (S-17)
RCA	7029	10	19	22	.49		1.1-15	Dormer (S-17)

Table 7b

Short Wavelength Photomultipliers

CsNaKSb (Multialkali)

Type	Make, Model,	Stages	d., mm	$QE_{\%pk}$	$\lambda_{\mu pk}$	$\lambda_{\mu 1/2}$	NEP at 300°K watts/cps$^{1/2}$	Remarks
S-20					.42	.6		
AMP	XP1117	9	14	18.			5-15	Ruggedized
EMI	9558B	11	44	20			2.1-16	
EMR	541E-01-14	14	25	25			6-17	Potted
ITT	FW-143	16	2.5	19			1.1-15	Ruggedized
Non-std								
EMI	9558Q	11	44	23	.26/.42		2.1-16	
EMR	541E-05M-14	14	25	25	.42		6-17	Potted, UV
ITT	F4013 sapp.	16	2.5	12	.45		5.8-15	UV
ITT	F4003 mod.		2.5x19	28	.52		-	Mult. Total Reflection
RCA	C70038D	10	13x16	35	.39/.54		-	Dormer S-17

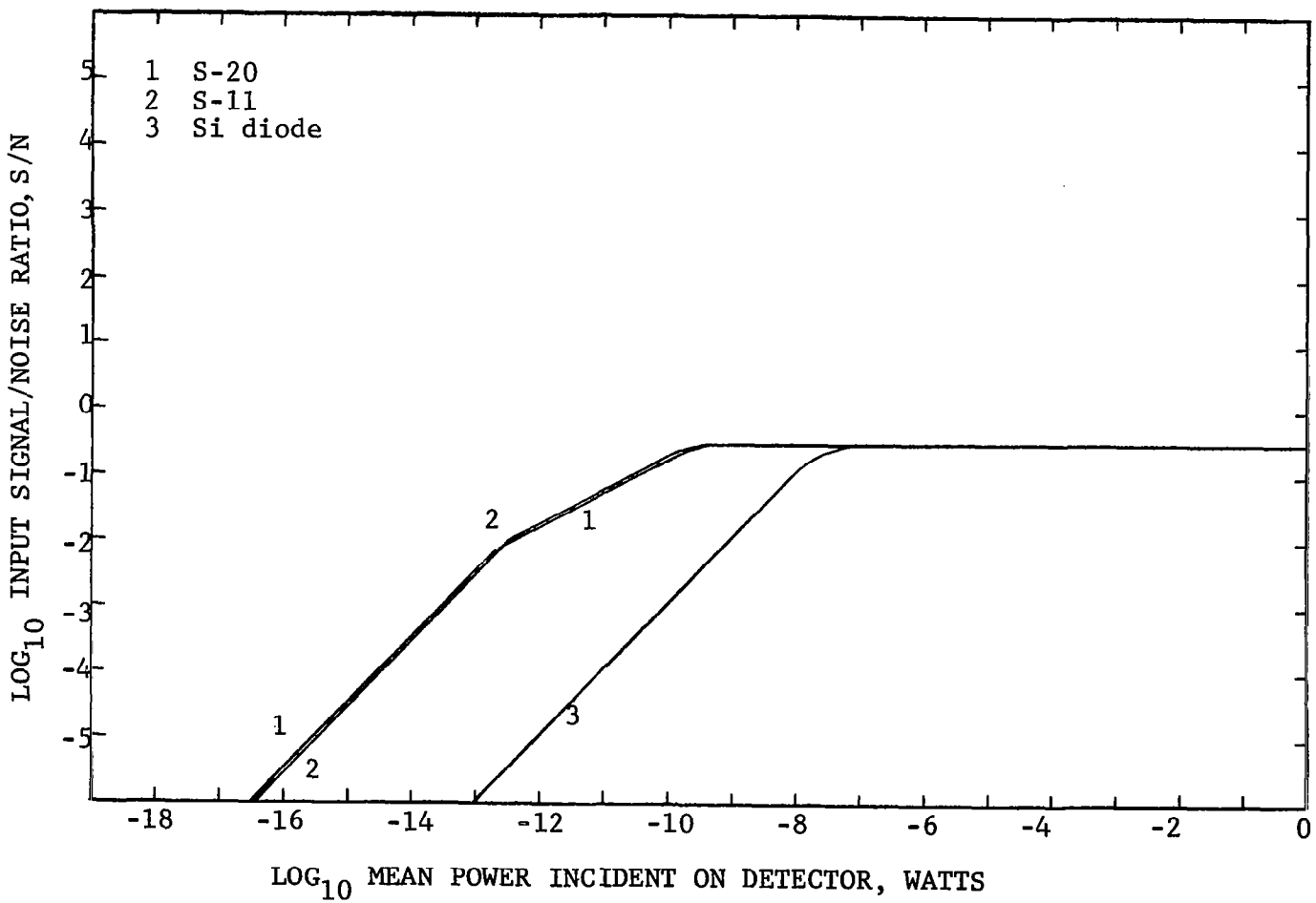

Fig. 8 Dominant Noise Terms for Visible Light Detectors, 4000A

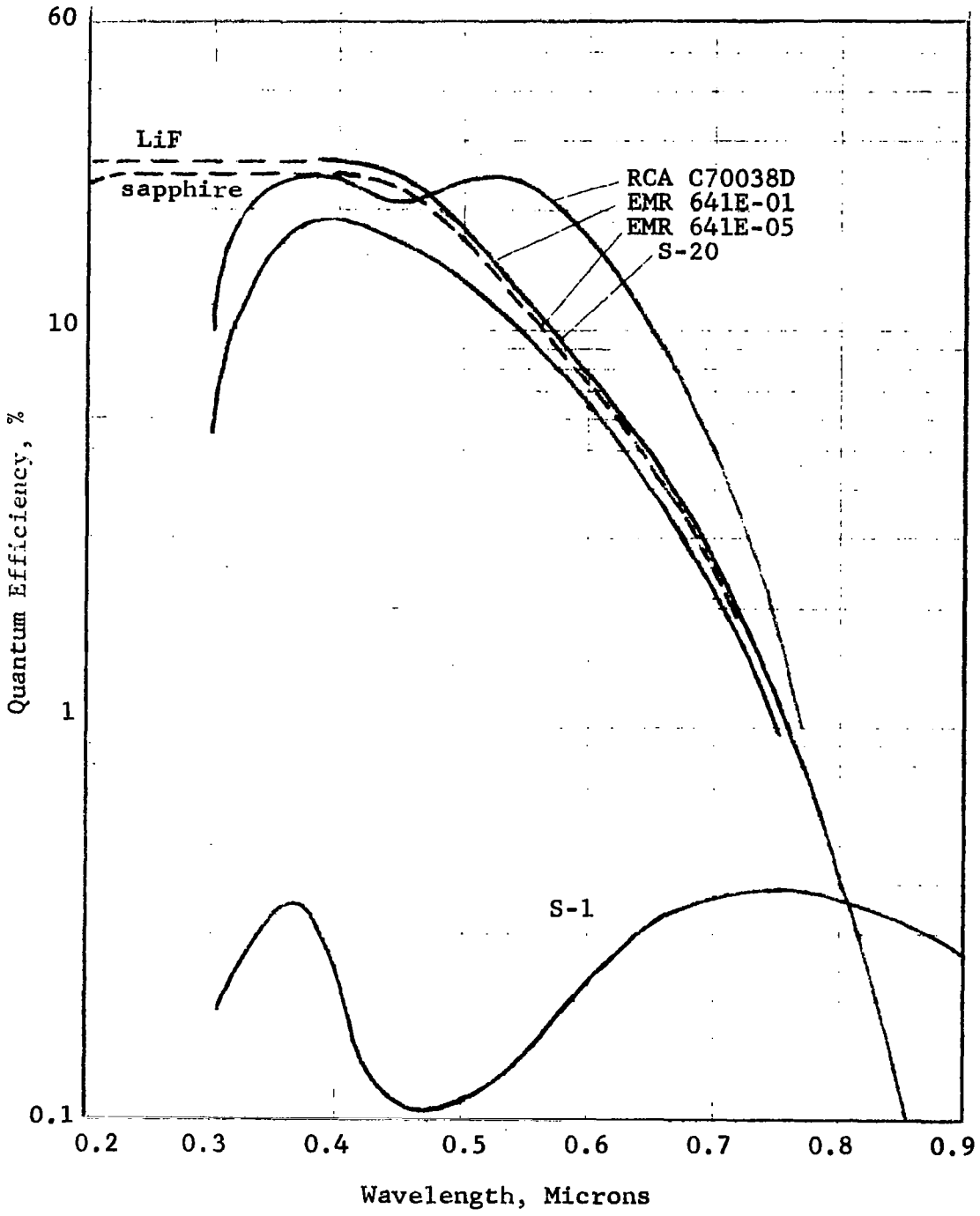

Fig. 9 Variants of the Multialkali Photocathode

fluoride window in place of the 7056 glass. It has also been redrawn at 1.08 times lower quantum efficiency throughout to show the reflectance loss effect of a sapphire window. The sapphire window version is available on special order as No. 641E-05-18. The lithium fluoride-opaque multialkali combination is not yet available. In the multialkali cathode, response at wavelengths longer than 0.6 microns can be increased further, at the price of increased dark current, by an increase in cesium content. The RCA tube shows a second peak at 0.53 microns, and is offered for detecting "low-level light in relatively high background brightness" in laser applications, wherein we note dark current to be of secondary importance.

A preliminary announcement has been made by ITT Industrial Labs. of an extension of the reflection enhancement principle in which light is introduced through the edge of a thick glass window that has been cut to the appropriate angle. The light reflected from the cathode film is totally reflected within the glass for a second incidence. Quantum efficiency improvement factors of 2.5 and 3.5 at 5230 and 6943A, respectively, were reported. These correspond to approximately 28 and 8 percent. The corresponding efficiencies for the single-reflection RCA tube are 24 and 5.5 percent.

1.4.2 0.55 to 1.1 Microns

Detectors for this range are given in Table 8. The response of most of the photocathodes falls sharply beyond 0.5 microns. The S-1 and S-20 responses are the two important exceptions. The standard S-20 quantum efficiency peak is 20% at 0.4 microns, and down to 4.3% at 0.65 microns. The silicon diode is 56% at this wavelength. Figure 10 shows that the high diode detector noise prevents the utilization of the 13-fold efficiency advantage at 3% uncorrelated turbulence. Extension of the partial signal/noise ratios $S/(N_{ss}^2 + N_d^2)^{1/2}$ has been included in Fig. 10 in the area above S/N = 1, in order to display the mean intensity (7×10^{-8} watts) at which the partial curves for the two detectors cross. This point occurs approximately 1.5 cm($10^{3/2}$x) above the S/N = 0.1 ordinate representing minimum useful intensity for M_u = 3.16%. Therefore, the diode has an advantage for $M_u <$ 0.1%, if intensities greater than 7×10^{-8} watts are available.

At 0.8 microns the S-20 surface has a lower quantum efficiency than that of the S-1 which, in turn, is only 0.4%. The diode is up to 66%, a factor of 165. From Fig. 11, the detector crossover is seen to coincide with the point at which turbulence limiting occurs, 5.5×10^{-9} watts. Therefore, the diode has an advantage for $M_u <$ 3.16%, if intensities greater than 6×10^{-9} watts are available.

Table 8

Red and Near Infrared Detectors

Type	Make, Model,	Stages	d., mm	QE $\%_{pk}$	$\lambda_{\mu pk}$	$\lambda_{\mu 1/2}$	NEP w/cps$^{1/2}$	T °K	Remarks
S-1					.80	.96			
AMP	XP1116	10	14	0.3			1.2-12	300	
DUM	K1404	6	13	0.164			-	300	Potting Avail.
EMI	9864B	11	44	0.5			1.8-13	300	
ITT	FW-142	16	2.5	0.4			9-13	300	Ruggedized
ITT	FW-142	16	2.5	0.4			3-17	196	
RCA	7102	10		0.4			1.7-12	300	
Si Photodiode									
EGG	SD-100	-	2.5	35	.9		1.0-12	300	Obsolete 7/66
EGG	SGD-100	-	2.5	70	.9		7.9-13	300	Rugged
EGG	SGD-444	-	11	55	.9		1.9-12	300	Rugged
ENL	612B		5	-	1.06	1.14	9-14	300	Rugged
TXI	SIV		1.4	60	0.9	1.04	3.5-13	300	Rugged
UDT	PIN-10		20	$>$ 30	0.85	1.05	$<$ 1-11	300	Rugged

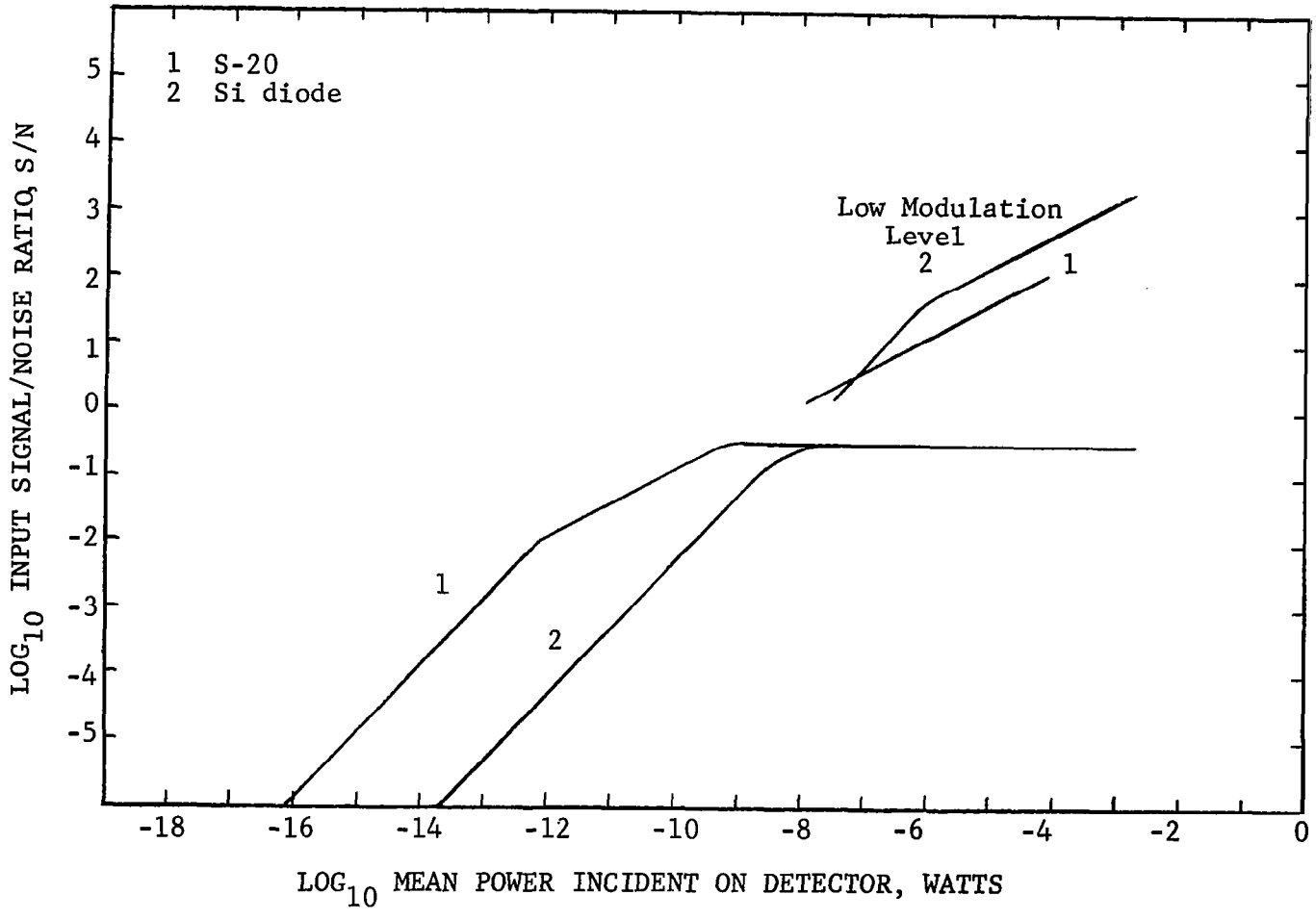

Fig. 10 Dominant Noise Terms for Visible Light Detectors, 6500A

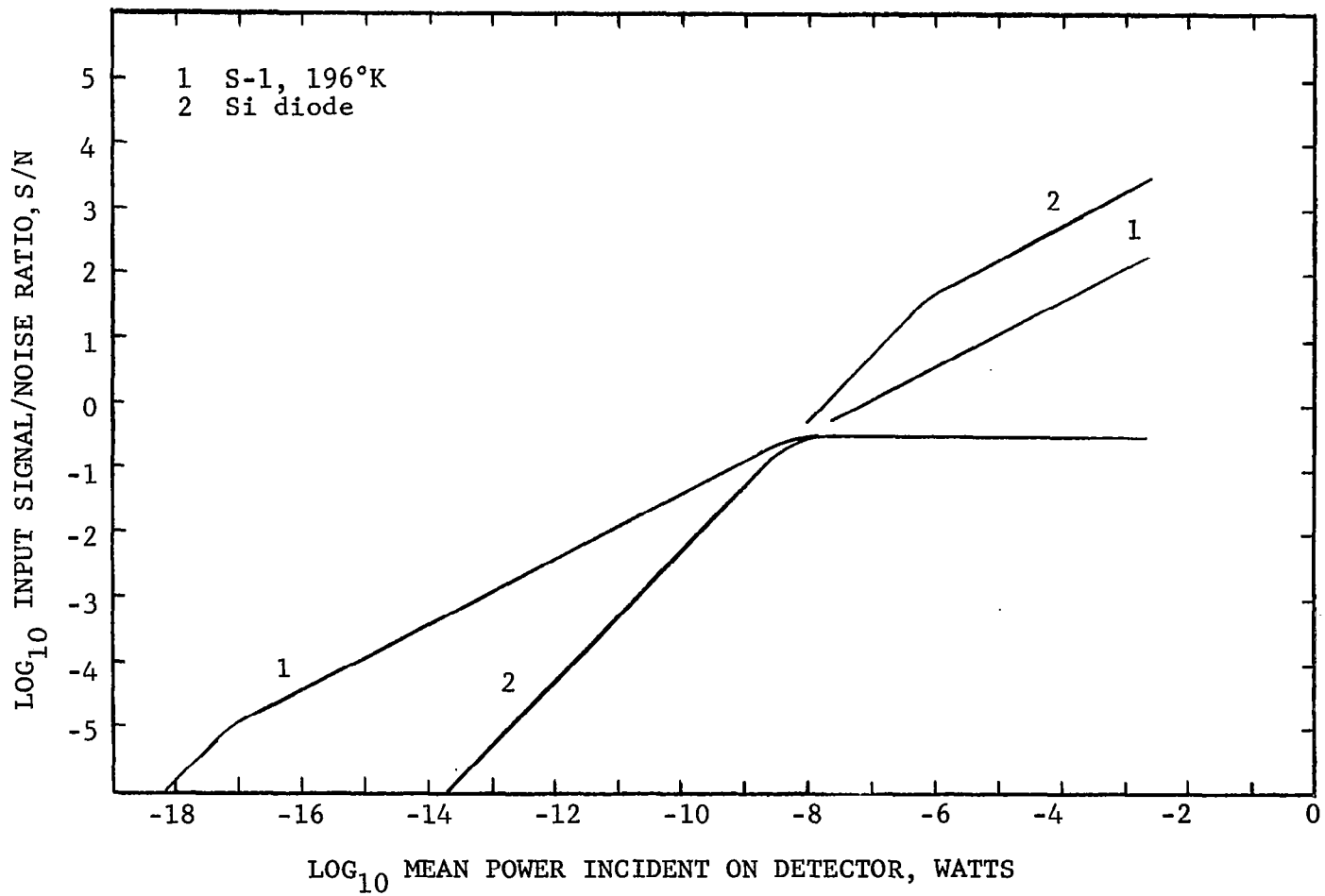

Fig. 11 Dominant Noise Terms for Near-Infrared Detectors, 8000A

Again, it should be noted that there is nothing sacrosanct about 1% correlated fluctuation and 3.2% uncorrelated fluctions which are used in the above discussion and on which the graphs are based. Provided the user understands how ultimately, for some input light intensity, we will reach a flow noise limited situation, the graphs may easily be interpreted for any other known conditions.

1.4.3 1.1 to 5.5 Microns

The three types of detectors most applicable to this range are lead sulfide, indium arsenide, and indium antimonide. Makes and models are given in Tables 9a, 9b, and 9c, respectively. As one might suppose, recent developmental detectors submitted to NOLC are higher in detectivity than the models on the market. D* values quoted in the table are guaranteed minima. For the graphs, typical values were taken. For all detectors, minimum and maximum detectivities tend to be a factor of two on either side of the typical value. Some manufacturers offer a factor of two above and below average, priced accordingly. Thus, in general, variations within a factor of two in the tables among different makes should not be made a basis of choice.

Comparison of the three types is made at 3 and at 3.5 microns, in Figures 12 and 13, respectively. The lead-salt detectors are unusual in having a long-wave spectral cutoff that increases with decreasing temperature. The wavelength 3.5 microns happens to be rather inaccessible to room-temperature lead sulfide and to cooled indium arsenide. It also

TABLE 9a

LEAD SULFIDE, PC MODE

Temp °K	Manuf.	Model	D^*_{pk} $X10^{-10}$	τ μsec	$\lambda_{1/2}$ μ	S(λ) Type	1a SEN WB,.05	1b N(f) Type	2 dyn. range μ watt	3 f_{3db} kc/s	4 $A^{1/2}_{mm}$
300	K		10	250	2.5			1/f		0.6	
195	K		17	455	3.0			1/f		.35	
77	K		8	455	3.3			1/f		.35	
300	EK	N	7	500-1000	2.7	~EQ	~400	1/f		.15-.3	0.07-100
300	EK	O	5	200-500	2.7	EQ		1/f		.3 -.8	.07-7
300	EK	P	1.8	50-100	2.9	EQ		1/f		1.5 - 3	.07-7
195	EK	P	17	2000-4000	3.8	EQ		1/f	0.15	.04-.08	.5
300	SBRC		8	300	2.8	EQ	<1000	1/f		0.4	0.05-10
195	SBRC		40	3500	3.2	EQ	<1000	1/f		.05	0.05-10
77	SBRC		10	3000	3.6	EQ	<1000	1/f		.06	0.05-10
77	SBRC	#E-1-9[1]	54	1800	4.0	EQ	20	1/f		.09	1.7

[1]NOLC sample

TABLE 9b

INDIUM ARSENIDE

Mode	Temp °K	Manuf.	Model	F.O.V. deg	D^*_{pk} X10-10	τ μsec	$\lambda_{1/2}$ μ	S(λ) Type	1a SEN WB,05 pw	1b N(f) Type	2 dyn. range WB	3 f_{3db} kc/s	4 $A_{nm}^{1/2}$
PEM	295	K		180	0.014	0.2	3.4		80,000	TH			
PV	295	K		180	.25	<2	3.7		4,500			>75	
PV	300	TXI	IAV	180	.29	<0.5	3.6	EQ	3,800	150WH		>300	0.5-3d
PV	196	TXI	IAV	180	20.	<0.5	3.4	EQ	56	150WH		>300	0.5-3d
PV	77	TXI	IAV	180	25.	<0.5	3.1	EQ	45	150WH		>300	0.5-3d
PV	300	ENL	632	180	.1	1	3.2	EQ					2d
PV	77	ENL		30	1.								2d
PV	216	SBRC		180	3.5	<2	3.4	EQ				>75	1-2
PV	193	SBRC		180	12.	<2	3.4	EQ	95	1/f350WH		>75	1-2
PV	77	SBRC		180	26.	<2	3.1	EQ		1/f1900WH		>75	1-2
PC	295	K			0.014	0.2	3.4						

TABLE 9c

INDIUM ANTIMONIDE

Mode	Temp °K	Manuf.	Model	F.O.V. deg	D^*_{pk} X10^{-10}	τ μsec	$\lambda_{1/2}$ μ	S(λ) Type	1a SEN WB,.05 pw	1b N(f) Type	2 dyn. range WB	3 f_{3db} kc/s	4 $A^{1/2}_{mm}$
PEM	298	K		180	.03	0.2	7.0			TH			
PEM	298	ENL	649	180	0.003	<1	6.9	~EQ				>150	.5-1
PEM	298	RE('59)[1]	A-04	180	.007	<1	7.0						
PV	77	K			4.3	<1	5.6						
PV	195	ENL		180	0.9min	<1	6.1	EQ	1400	1/f2000BL		>150	.9-1.7
PV	77	ENL		180	2.0min	<1	5.5	EQ	570	1/f500BL		>150	
PV	77	ENL	647A	180	5.7	<1	5.5	EQ				>150	
PV	77	ENL	647B	180	6.8	<1	5.5	EQ				>150	
PV	77	ENL	647C	180	9	<1	5.5	EQ				>150	
PV	77	TXI	ISV-A	180	8.8	<1	5.5	EQ	130	1/f80BL	~10^4	>150	.1-1
PV	77	TXI	ISV-A	50	18.		5.5	EQ					
PV	77	AVCO		180	>5		5.5	EQ					.25-.5
PC	77	K		60	6	<2	5.5					>75	
PC	77	ENL	648A		5.7		5.5						0.25-0.5
PC	77	ENL	648B		6.8		5.5						
PC	77	TXI	ISC	180	5.5	10	5.5	EQ			>200	25	
PC	77	TXI	ISC	50	7.7	15						10	
PC	77	SBRC		180	4.6	<10	5.5	EQ				>15	0.7
PC	77	HW('61)[2]	DLG67C	180	9.0	<5	5.3	EQ					0.3-3

[1] Radiation Electronics Corp. (1959)

[2] Honeywell (1961)

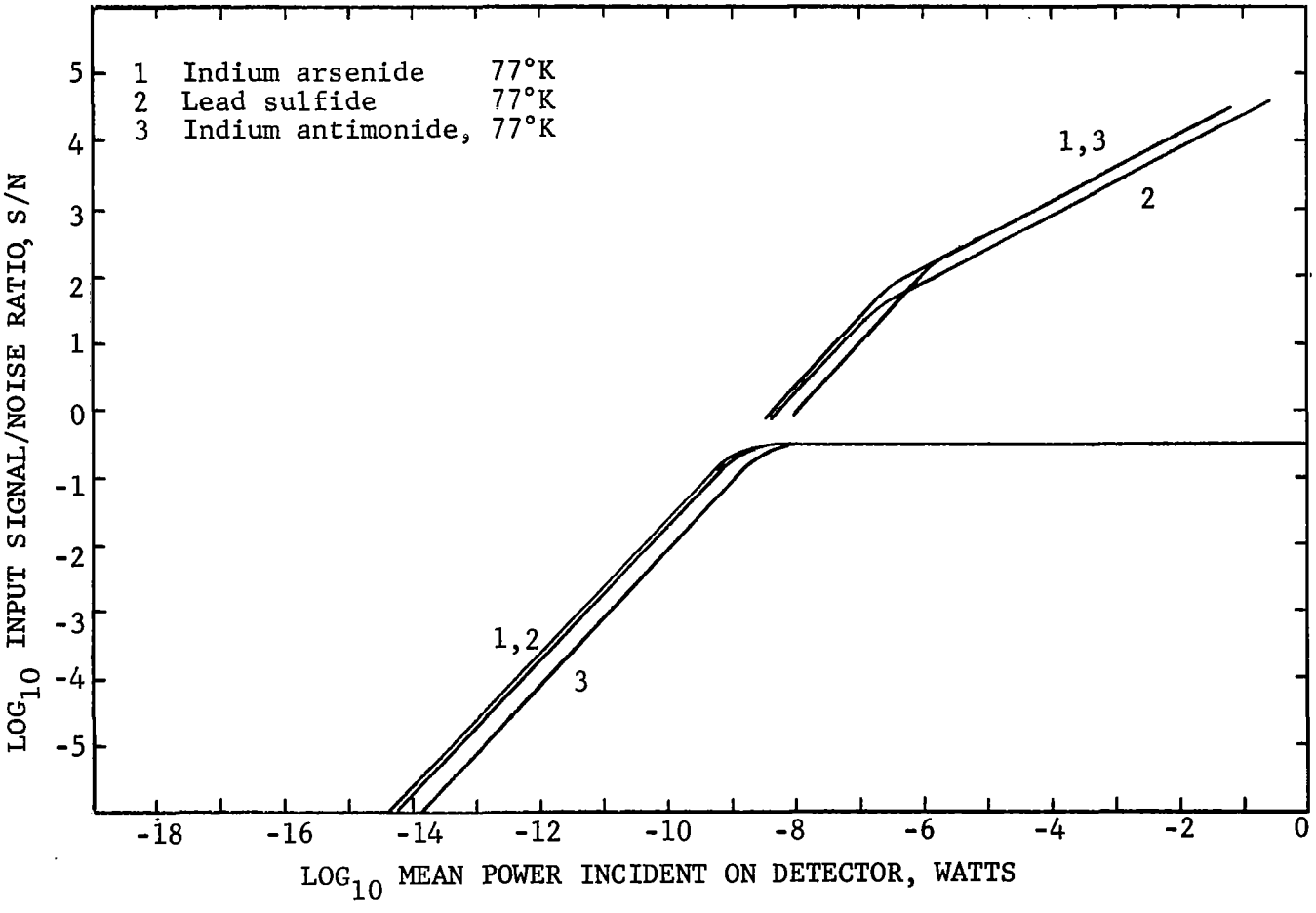

Fig. 12 Dominant Noise Terms of Intermediate Infrared Detectors at 3.0 Microns

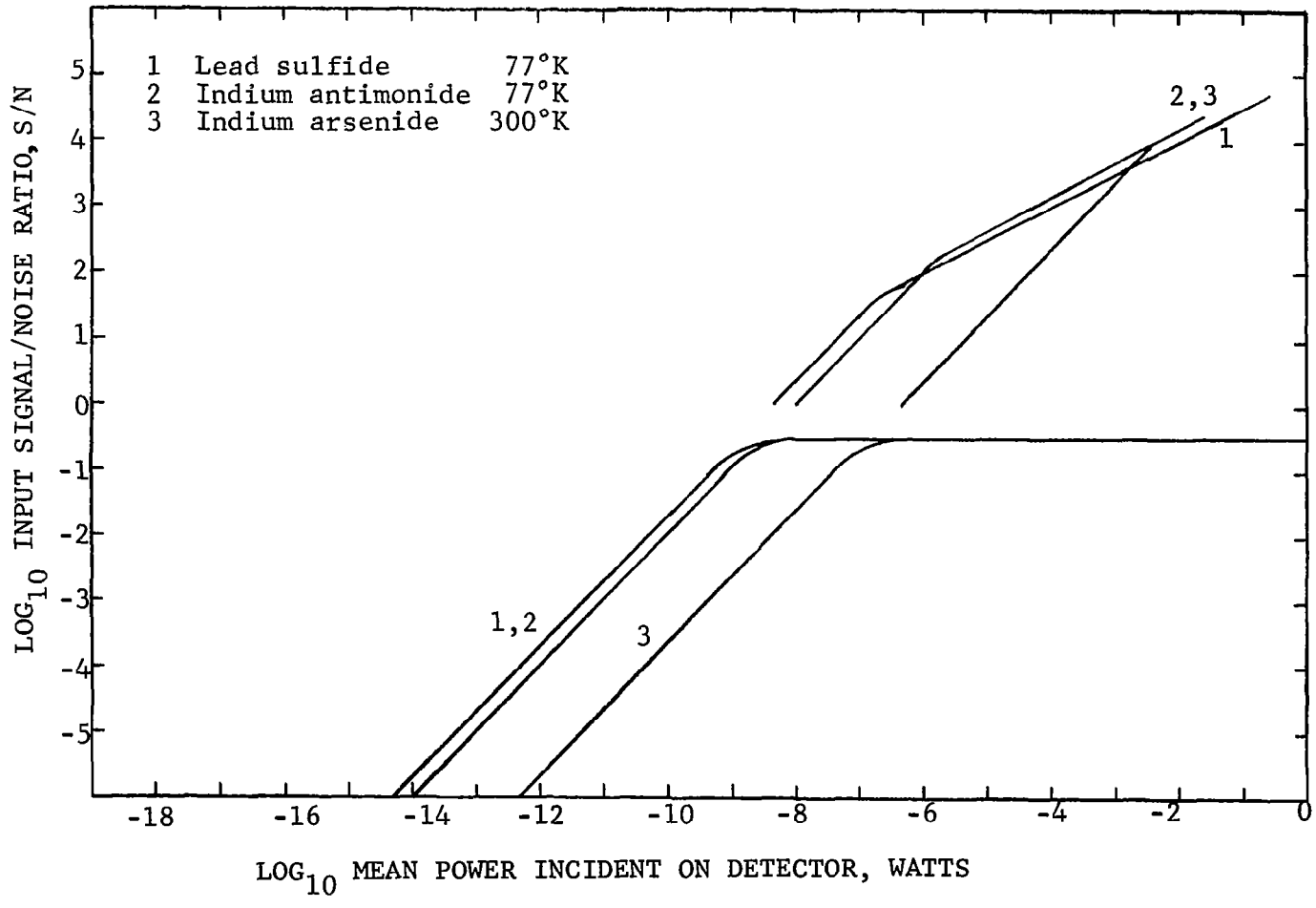

Fig. 13 Dominant Noise Terms of Intermediate Infrared Detectors at 3.5 Microns

happens to be in the narrow region occupied by the intense absorption bands due to the stretching modes of carbon-hydrogen present in all hydrocarbon compounds. Therefore, Figure 13 was plotted for PbS at 77°K and InAs at 300°K, while Figure 12 shows InAs for 77°K. At 3 microns, these detectors are detector-noise limited below 5 x 10^{-7} watts (Φ_{ssd}); a typical mean detector input at 3 microns and $\lambda/\Delta\lambda$ = 1000 for an infrared grating spectrometer using a Nernst glower source is 6 x 10^{-7} watts. All three types become turbulence-noise limited at a factor of a hundred below this value. Therefore, with a focused beam system, unusually high or M_u much less than 1%, an indium antimonide detector would appear to cover the range from 1 to 5.5 microns satisfactorily with the customary infrared sources. The room-temperature indium arsenide requires 1.5 x 10^{-7} watts to become turbulence noise limited; it is of marginal interest.

Lead sulfide has a small advantage over indium antimonide at wavelengths less than 3 microns, but it has a long time constant requiring electrical equalization. Equalization is feasible and routine, but the time constant is highly temperature dependent, and thus correlation detectors must be maintained at matched as well as fixed absolute temperatures. Figure 3 shows frequency dependence data obtained by NOLC on a lead sulfide detector. The signal and noise are seen both to vary inversely with frequency above 100 cps. The noise is predominantly generation-recombination noise N_{gr}. Thus, the

detectivity curve, a reduced signal/noise ratio plot, is independent of frequency to 40 kc/s. Since the high S/N prevailing below the 100 cps cutoff is maintained to 40 kc/s, the cutoff does not remotely represent the useful frequency limit. Equalization provides flat response to at least 40 kc/s at high S/N. The equalization introduces a calculable and measurable delay time that is no problem.

The indium antimonide detector shown does almost as well in S/N and, because of its fast response, has no temperature-phase matching problems. The indium antimonide performance approaches the lead sulfide in part because the InSb data are for a detector restricted to a 50-degree field of view, chosen to be compatible with an f/7 spectrometer followed by 6:1 demagnification. A factor of 2 is realized over a 180° field of view for InSb. The lead sulfide data, on the other hand, are for a 180° field of view because, although improvement at low frequencies is possible with field restriction, the detectivity is thermal noise limited at high frequencies. A calculation indicated that the thermal noise in the lead sulfide detector-load resistor system lies not far below the dominant gr noise, and the detectivity is not flat much beyond 50 kc/s. A decrease in background shot noise greater than two-fold would result in thermal-noise limiting below 50 kc/s with consequent loss in S/N.

1.4.4 5.5 to 21.5 Microns

For fast response and highest detectivity in this region, extrinsic germanium detectors are required. Several inpurity activators are available to provide various compromises between spectral cutoff and peak detectivity. Detectivities can be described fairly well as proportionalities with wavelength up to a maximum at the cutoff. Departures are introduced by means of antireflection coatings to favor selected regions. Particular makes and models are listed in Table 10. Germanium:copper and germanium:cadmium extend just beyond 20 microns. Germanium: copper seems to offer a small advantage in detectivity where the same manufacturer offers both. The model selected for the data in Table 6 is vibration isolated to minimize microphonics. These detectors are comparatively large, e.g., 4-1/2-inch in diameter x 14 inches in length, because of the inclusion of a liquid helium dewar contained in a liquid nitrogen dewar.

It should be noted that, for extrinsic detectors, effective area means the area of an aperture in a cooled cavity within which the sensitive crystal element is housed. This arrangement is necessitated by the generally low absorbance of extrinsic semiconductors. Multiple incidence is required to bring the detective quantum efficiency up to 0.5 times the window transmittance. In Table 6 window transmittance is 0.7 for the KRS-5 window of the QRN1009 detector.

TABLE 10

EXTRINSIC GERMANIUM, PC MODE

Type	Temp °K	Manuf.	Model	Window	F.O.V. deg	D^*_{pk} $X10^{-10}$	τ μsec	$\lambda_{1/2}$ μ	S(λ) Type	1a SEN WB,0.5 pw	1b N(f) Type	2 dyn. range WB	3 f_{3db} kc/s	4 $A^{1/2}_{mn}$
Ge:Au		K				1.75	<1	7.1		640	40WH			
Ge:Au	78	RAY	QKN1004	BaF_2	90	.75	<1	7	2pks.	1500	$1/f^{2+}$150WH		>150	2d
Ge:Au	77	SBRC		Si(5μ)	180	.37	~1	8	2pks.	3000	WH		~150	2d
Ge:Hg	35	RAY	QKN1266	BaF_2	45	.4	<1	13.5	EQ	2800	BL		>150	0.5
Ge:Hg	<21	SBRC		1RT2	150	.7	~1		~EQ	1600				.5-5d
Ge:Hg	<21	SBRC		1RT2	60	1.3	~1	10.5	~EQ	860				.5-5d
Ge:Hg	<20	TXI	GHC	1RT2	120	1.6	<0.1	13.9	EQ		BL		>1500	<0.45
Ge:Hg	<20	TXI	GHC	1RT2	90	2.0	<0.1	13.9	EQ		BL		>1500	<0.45
Ge:Hg	<20	TXI	GHC	1RT2	80	2.2	<0.1	13.9	EQ		BL		>1500	<0.45
Ge:Hg	<20	TXI	GHC	1RT2	40	4.1	<0.1	13.9	EQ		BL		>1500	<0.45
Ge:Hg	<20	TXI	GHC	1RT2	20	8.0	<0.1	13.9	EQ		BL		>1500	<0.45
Ge:Cd	<25	K				1.8		21.5		620	1/f500BL			
Ge:Cd	<25	RAY	QKN961	BaF_2		1.2	<1			930			>150	
Ge:Cd	<25	RAY	1007	KRS5		1.4	<1			800			>150	
Ge:Cu	<20	K				2.5		27		450				
Ge:Cu	5	RAY	QKN902[1]	BaF_2	90	1.7	<1	15	~EQ	660	BL		>150	.5,1,2
Ge:Cu	5	RAY	QKN1009	KRS5	90	2.1	<1	25	~EQ	530	BL		>150	.5,1,2
Ge:Cu	<14	SBRC		KRS5	60	2.5min	<1	24	EQ=kλ	450	WH		>150	.5-5d
Ge:Cu	5	TXI	GCC	1RT4	180	.87	<0.1	25	EQ	1300	BL		>1500	.3-3d
Ge:Cu	5	TXI	GCC	1RT4	120	1.0	<0.1	25		1100	BL		>1500	.3-3d
Ge:Cu	5	TXI	GCC	1RT4	90	1.25	<0.1	25		890	BL		>1500	.3-3d
Ge:Cu	5	TXI	GCC	1RT4	60	1.75	<0.1	25		640	BL		>1500	.3-3d
Ge:Cu	5	TXI	GCC	1RT4	30	3.25	<0.1	25		343	BL		>1500	.3-3d

[1] 5K BaF_2 filter

2. SPECIFIC DETECTOR CHOICES

Because of more varied applications, there is more diversity on which to base choice among photomultiplier detectors than among infrared semiconductor detectors. Most of the latter have been developed for military applications broadly similar in signal processing problems to the crossed-beam application. They are offered with a wide choice of area, field of view, and packaging. A very few manufacturers dominate the field, and they are competitive. The choice of the optimum detector on the basis of detectivity is rather arbitrary, since the actual performance of a detector may vary over a considerable range. It is commonplace to list minimum, typical, and maximum values of detectivity for each detector, where the ratio of maximum to minimum detectivity is typically of the order of 4. There is considerable overlap between the ranges quoted by different manufacturers for similar detectors. Also, for a premium price, most manufacturers will select a detector of unusually high detectivity, usually about twice the typical value.

With the qualifications noted above borne in mind, the detector choices are listed in Table 11. The applicable spectral range is indicated by brackets for each detector. The spectral detectivity is indicated in Figure 14, where a log-log plot has been made of the wide-band detectivity $D_{\Delta f}$ against wavelength. The region least effectively covered is between 5.5 and 10 microns. A germanium:mercury detector would

TABLE 11

SPECIFIC DETECTORS

λ Microns	Mode	Type	Q.E.,%	Make	Model
0.15					
0.35	PM	CsSb	14	EMR	541A-05M
0.5					
	PM	Trialkali,S-20	20	EMR	641E-05-18
0.6					
	Photodiode	Si	70	EG&G	SGD-100
0.75					
	PM	CsAgO,S-1	0.4	ITTIL	FW-142
1.1					
	PC	Lead sulfide 300°C		EK	P
2.8				SBRC	no code
	PV	Indium arsenide 300°C		TXI	IAV-180°FOV
3.6					
	PV	Indium antimonide		TXI	ISV-A50°FOV
				ENL	647B
5.5				SBRC	LTO-50°FOV
	PC	Ge:Cu, KRS-5 window		RAY	QNK1009-90°
				SBRC	KRS-5-50°FOV
				TXI	GCC-60°FOV
21.5					

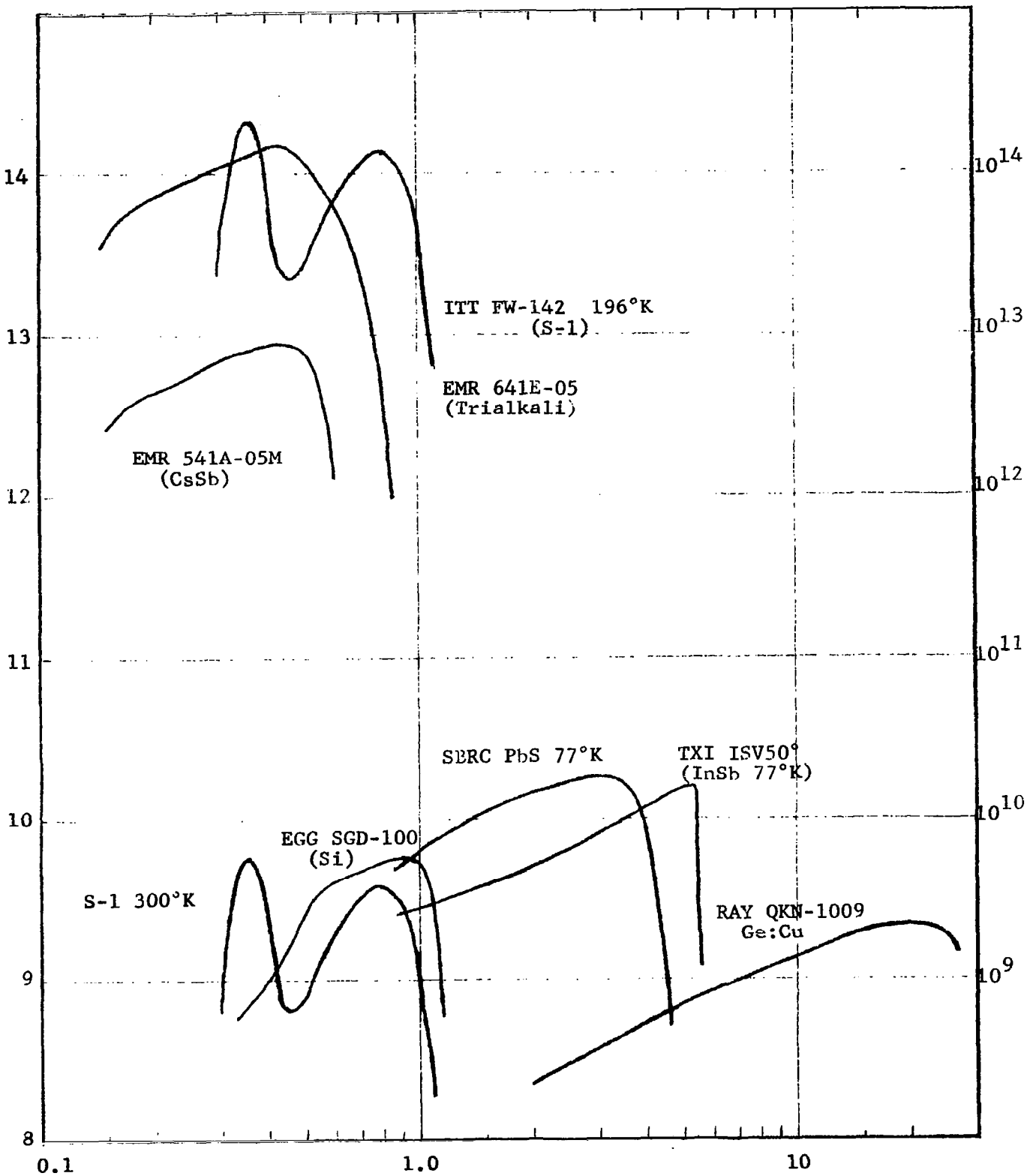

Fig. 14 Spectral Detectivity of Selected Detectors

increasing detectivity in this region by a factor of two over termanium:copper with the same qualifying conditions applicable to both, such as field of view, window choice, area, and packaging. Figure 14 is relevant, however, only if the mean intensity is low enough that the signal is not uncorrelated-turbulence limited or signal-shot-noise limited.

The CsSb detector listed in Table 11 is the one presently employed. Substitution of one of the enhanced S-20 detectors of Figure 9 would provide a factor of 1.8 increase in quantum efficiency from 0.185 to 0.4 microns. The S-1 multiplier recommended is one of 0.1 inch effective diameter, designed for refrigeration in star tracking applications. Because of its small effective diameter and other constructional features, the low temperature dark current noise is unusually small. The recommended silicon diode is designed for speed and linearity in laser detector applications. However, its special guard ring construction also limits dark current to values acceptable in cross beam applications. Although the diode detector noise is greater than the S-1 signal shot noise below 10^{-6} watts, the diode signal/noise ratio is the greater above 5.5×10^{-9} watts because of high quantum efficiency. Therefore the SGD-100 diode was chosen among diodes on the basis of its 70% quantum efficiency, flat frequency response and low price rather than its detectivity. The lead sulfide and indium arsenide detectors were included because they offer the convenience of room temperature operation with fairly high detectivity. Matched equalization and temperature control are required, however.

The emphasis in this report has been on detectivity or quantum efficiency as criteria of choice among detectors because one or the other expresses relative precision of measurement. Where available intensity permits a choice, however, other parameters may be used, such as vibration immunity and surface homogeneity of responsivity. The parameter most difficult to specify in advance is operability in an environment of high acoustical noise. Detectors are rated quantitatively for their ability to withstand severe shock and vibration without permanent damage, but little is known about performance in such an environment. Detectors that operate in low-impedance circuits may be expected to tend to show less disturbance; thus, a large current gain permits the use of a small load resistance. Examples are many dynodes for photomultipliers, and large carrier mobility for photoconductors, notably indium antimonide.

Another parameter for which little information is available is homogeneity of responsivity of the detector surface. This quantity varies as much as a factor of two from point to point for semiconductor detectors. Figure 15 shows a responsivity contour map of a lead selenide detector, obtained by Potter, Pernett and Naugle[15] at NOLC, by means of a scanning light spot 0.066mm in diameter. The extrinsic germanium detectors are presumably an exception in view of their blackbody cavity construction. Here the effective detector surface is the aperture of the cavity. Eastman Kodak suggests a small field lens in front of their lead sulfide detector to eliminate

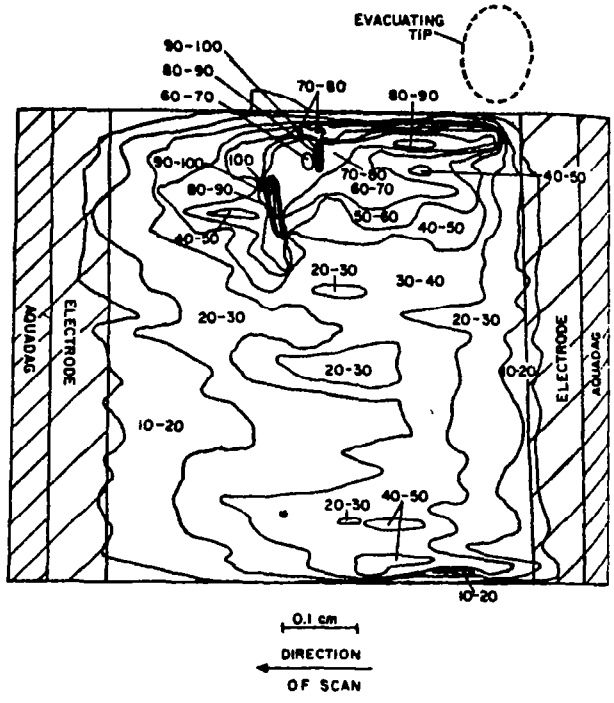

Fig. 15 NOLC Responsivity Contour of a Lead Selenide Detector

scanning noise due to motion of a sharply focused moving image on the detector. The image is focused on the lens. The customary spectrometer arrangement, where the stationary exit slit is imaged on the detector, achieves the same result.

REFERENCES

1. Fisher, M.J. and Krause, F.R., "The Crossed Beam Correlation Technique," Journal of Fluid Mechanics (to be published)

2. Krause, F.R., Montgomery, A.J., Davies, W.O. and Fisher, M.J., "Optical Methods of Remote Sensing of Local Thermodynamic Properties and Turbulence," NASA TMX (to be published)

3. Rose, A., "Advances in Electronics I," 131-166 (1948)

4. Jones, R.C., "Advances in Electronics and Electron Physics," Vol. XI, 87-183 (1959), Academic Press, N.Y.

5. Shockley, W.R. and Pierce, J.R., Proc. I.R.E. 26, 321-32 (1938)

6. Faber, Kruse and Saur, J. Opt. Soc. Am. 51, 115 (1961)

7. Goucher, F.S., Phys. Rev. 78, 816(L) 1950.

8. Rose, A., Proc. I.R.E. 43, 1850-1869 (1955)

9. Jones, R.C., "Advances in Electronics and Electron Physics, V," p. 1, (1953), Academic Press, N.Y.

10. Garbuny, M., Vogl, T.P. and Hansen, J.R., Rev. Sci. Inst. 28, 826 (1957)

11. Eisenman, W.L., Batts, R.L. and Merriam, J.D., Opt. Soc. Am. 53, 729 (1963)

12. Kruse, P.W., McGlauchlin, L.D. and McQuistan, R.B., "Elements of Infrared Technology, Wiley, N.Y., 1962.

13. Levinstein, H., "Applied Optics and Optical Engineering II," R. Kingslake, ed., Academic Press., N.Y., 1965, p327.

14. Bendat, J.S., "Principles and Applications of Random Noise Theory," Wiley, N.Y., 1958, p274.

15. Potter, R.F., Pernett, J.M. and Naugle, A.B., Proc. I.R.E. 47, 1503 (1959).